1   **An Assessment of Antarctic Sea-ice Thickness in CMIP6 Simulations with Comparison to the**
2   **Satellite-based Observations and Reanalyses**

3

4   **Shreya Trivedi[1], Will Hobbs[2], and Marilyn Raphael[1]**

5

6   [1]Department of Geography, University of California, Los Angeles

7   [2]Australian Antarctic Program Partnership, Institute for Marine and Antarctic Studies,
8   University of Tasmania, nipaluna/Hobart, Australia

9

10   **Corresponding author:** Shreya Trivedi (shreyatrivedi26@ucla.edu)

11 **Abstract**

12 Sea-ice thickness, though critical to our understanding of sea-ice variability, remains relatively
13 understudied compared to surface sea-ice parameters in the Southern Ocean. To remedy this, we
14 examine spatio-temporal variations in sea-ice thickness by analyzing historical simulations from
15 39 coupled climate models in CMIP6, comparing them with three sea-ice products, including
16 satellite-derived observations and reanalyses. Furthermore, we compare seasonal trends in
17 simulated sea ice thickness with trends in sea ice area. Our results indicate that CMIP6 models
18 can replicate the mean seasonal cycle and spatial patterns of sea-ice thickness. During its
19 maximum in February, these models align well with satellite-based observation products.
20 However, during the annual minima, CMIP6 models show significant agreement with the
21 reanalysis products. Certain models exhibit unrealistic historical mean states compared to the
22 sea-ice products resulting in significant inter-model spread. CMIP6 models can simulate sea-ice
23 area more accurately than the sea-ice thickness. They also simulate a positive relationship
24 between the two parameters in September such that models with greater area tend to exhibit
25 thicker ice. In contrast, there is a negative relationship in February when greater area is associated
26 with lower thickness since only the thicker ice survives the summer melt. Moreover, our study
27 highlights significant positive trends in sea-ice thickness observed during the cooler seasons, which
28 are nearly absent in the warmer seasons where positive trends are predominantly observed in sea-
29 ice area. The spatial distribution of SIT biases is closely linked to uncertainties in modeling the ice
30 edge and the dynamic processes, emphasizing the need for better model representation of both. This
31 study, therefore, highlights the need for improved representation of Antarctic sea-ice processes in
32 models for accurate projections of thickness and related volume changes.

33

34 ## 1. Introduction

35 Antarctic sea-ice extent which showed a small positive linear trend since the start of the satellite
36 era (Cavalieri & Parkinson, 2008; Parkinson & Cavalieri, 2012; Turner et al., 2015; Zwally et al.,
37 2002), has decreased significantly since mid-2015 (Eayrs et al., 2021; Raphael and Handcock,
38 2022; Wang et al., 2022; Turner et al., 2022). Since there is a long and reliable observational record
39 available for the surface characteristics (such as extent and area) of the ice, they have been the
40 primary focus for understanding the variability in the sea-ice cover in the Antarctic. However,
41 complete understanding of the changes in sea-ice and their potential impact on climate (*via* a
42 variety of climate-sea-ice feedbacks) and marine ecosystems is not possible without an
43 understanding of the variability in sea-ice thickness (SIT) and volume (SIV) (Holland et al., 2006;
44 Stammerjohn et al., 2008).

45 SIV (*viz.* the product of both area and thickness) serves as a measure of total sea-ice production
46 and, hence, a measure of the surface salinity flux in winter, the freshwater input to the ocean in
47 summer, and total heat exchange with the atmosphere (Maksym et al., 2012). Understanding the
48 variability in SIV improves our understanding of surface buoyancy flux and its impact on the
49 ventilation of Southern Ocean deep waters, as well as trends and variability in salinity in the region
50 (Haumann et al., 2016; Abernathy et al, 2016; Pellichero et al., 2018). This understanding in turn,
51 informs our knowledge about global ocean heat and carbon uptake processes (Williams et al.,
52 2023).

53 SIT varies seasonally and is an important component of the Antarctic ice budget (Kurtz & Markus,
54 2012; Worby et al., 2008). SIT is important for the marine biology of the Antarctic ecosystem. It
55 affects the maximum biomass of algae in different ice layers, which in turn influences the food
56 web of the Southern Ocean. SIT, along with the snow depth, affects the light penetration and
57 availability for the phytoplankton contributing further to their production and bloom (Massom &
58 Stammerjohn, 2010; Schultz, 2013). Therefore, a long-term assessment of SIT/SIV in combination
59 with surface sea-ice characteristics, is important for a complete understanding of the ongoing
60 changes in the Antarctic sea-ice and its impacts (Massonnet et al., 2013; Sallée et al., 2023).

61 Among the currently available SIT datasets, ship-based observations from ASPeCt (Antarctic Sea
62 ice Processes and Climate) tend to underestimate mean measurements because ship routings
63 preferably avoid thicker sea-ice (Worby et al., 2008). Airborne electromagnetic data, NASA
64 Operation *IceBridge* (Koenig et al., 2010) and the upward-looking sonars (ULS) (Behrendt et al.,
65 2013) provide valuable spatio-temporal information but are limited to certain regions, lacking
66 circum-Antarctic distribution. To overcome some of the limitations, advanced retrieval techniques
67 in the form of satellite remote sensing, including passive microwave sensors for thin ice (Kurtz &
68 Markus, 2012), and active sensors like Synthetic Aperture Radar (SAR), have now been applied
69 to study circum-Antarctic SIT coverage and its long-term trends. More recently published satellite-
70 derived (both radar from Envisat-CryoSat-2 and laser from ICESat-2) altimetry-based SIT datasets
71 have proven to be the best source for circum-Antarctic SIT retrievals over the full thickness range
72 (Kurtz and Markus, 2012; Kacimi and Kwok, 2020; Wang et al., 2022). In general, gathering
73 Antarctic SIT data presents significant challenges owing to harsh weather conditions, extensive
74 snow cover, and intricate snow metamorphism processes. These factors introduce uncertainties in
75 both *in-situ* measurements and satellite altimetry observations, particularly concerning the
76 accuracy of detecting the snow-ice interface in the latter method. *In-situ* measurements like drilling
77 data are accurate but extremely limited in time and space and suffer from biases. We discuss such
78 uncertainties in detail in Sect.2.1.

79 Given the inconsistencies and limitations in the existing SIT observations, Global Coupled
80 Climate Models (GCMs) can serve as potentially valuable tools for assessing long-term SIT/SIV
81 variability and providing future projections. Hou et al. (2024) compared SIT simulations in CMIP6
82 models with radar altimetric datasets (Envisat-CryoSat-2) and identified common issues, including
83 lags and significant underestimation in SIT climatology during autumn and winter months, as well
84 as negative biases, particularly in the sea ice deformation zone around Antarctica. In an earlier
85 study, Trivedi et al. (2024) carried out a preliminary comparison of Antarctic SIT across CMIP6
86 models using *historical* simulations (1979–2014). However, that study only provided a brief
87 analysis of SIT trends and inter-model variability. A detailed assessment of model biases, seasonal
88 behavior, model performances in warmer scenarios and connections with other sea-ice parameters
89 is lacking. An assessment of the accuracy of SIT simulations in GCMs remains a challenge, which
90 adds to the *low confidence* in Antarctic sea-ice projections (Meredith et al, 2019). This is a key
91 motivation for our study.

92 In this study, we present a high-level evaluation of models in the Sixth Coupled Model
93 Intercomparison Project (CMIP6; Eyring et al., 2016) which simulate Antarctic SIT. We compare
94 these simulations to three different sea-ice products, including radar altimetric (as in Hou et al.,
95 2024) as well as two reanalysis (synthesis) datasets. Our results indicate that CMIP6 models can
96 reasonably capture the timing of the annual cycle and the spatial patterns in SIT, albeit with some

97 biases and model discrepancies, which we discuss. Notably, when compared to sea-ice area (SIA),
98 the models' performance remains suboptimal. This underscores the need for further improvements
99 in the representation of sea-ice dynamics and the physical processes controlling sea-ice-ocean
100 interactions in GCMs.

101 Since our understanding of historical sea-ice variability and the evaluation of climate models has
102 traditionally relied heavily on SIA records, this study extends the analysis by comparing simulated
103 SIT and SIV to SIA, in order to see how these diagnostics are related. Furthermore, we examine the
104 inter-relations between SIT and SIA during two key months to better understand their covariability.
105 We also identify significant seasonal trends in the three sea-ice parameters and analyze their
106 evolution over the selected time-period. These results emphasize the importance of incorporating
107 SIT metrics into future model evaluations to enhance our understanding of Antarctic sea-ice
108 dynamics and improve sea-ice and climate projections.

109

110 ## 2. Data and Methods

111 ### 2.1 Sea-ice products

112 Our study uses three different sea-ice records for SIT (Table S1): A dataset derived from Envisat-
113 CryoSat-2 (2002-2017; henceforth referred to as satellite product), the Global Ice-Ocean
114 Modeling and Assimilation System (GIOMAS, 1979-2014) and the German contribution to the
115 Estimating the Circulation and Climate of the Ocean project Version 3 (GECCO3, 1979-2014).
116 We compare them with the CMIP6 *historical* simulations which run until 2014. Since the satellite
117 products do not begin before 2002, our study focuses on the time-period between 2002-2014. To
118 eliminate mismatch in the spatial resolution, all the sea-ice products were regridded onto a
119 common CMIP6 model grid. SIA is calculated by multiplying the monthly values of sea-ice
120 concentration (SIC) by the corresponding grid cell area and summing over the Southern Hemisphere.
121 SIV was computed as the product of the actual floe thickness, SIC and the grid cell area, summed over the
122 circum-Antarctic region.

123 *SIT from Satellite Altimetry- Envisat and CryoSat-2:*

124 The Sea-Ice Climate Change Initiative (SICCI) project provides a large-scale Antarctic SIT dataset
125 from Envisat and CryoSat-2 with a 50 km spatial resolution (Hendricks et al., 2018a, 2018b). Both
126 Envisat and CryoSat-2 carry a radar altimeter based on the Ku Band frequency which is expected
127 to measure the ice freeboard (total freeboard minus snow depth), with spatiotemporal resolution
128 and spatial coverage consistent with each other. Our study utilizes the aggregated time-series data
129 from both satellites owing to the reasonable alignment of mean and modal values derived from
130 their radar freeboards throughout the sea-ice seasons (Hou et al., 2024; Schwegmann et al., 2016).
131 The SICCI dataset stands out as the most comprehensive satellite dataset spanning the circum-
132 Antarctic SIT from 2002 to present (Shi et al., 2021, Hou et al., 2024). This coverage is not
133 matched by more recent datasets like ICESat-2 (Xu et al., 2021). It is comparable to ULS-derived
134 SIT for the Weddell region (Shi et al., 2021; Liao et al., 2022; Wang et al., 2022) and aligns well
135 with *in-situ* ship-based observations (ASPeCt; Worby et al., 2008), showing highest thickness in
136 summers and lowest in autumn-winter.
137 Retrieval of such Antarctic SIT products is quite challenging and the existing satellite datasets are
138 not without uncertainties. Although the altimetric SIT measurements of Envisat and CryoSat-2

139 observations represent a major advancement in monitoring Antarctic SIT, it is an experimental
140 climate data record with uncertainties resulting from the inaccuracy in determining the snow–ice
141 interface (Willatt et al., 2010) and biases due to surface-type mixing and surface roughness
142 (Schwegmann et al., 2016; Paul et al., 2018; Tilling et al., 2019) resulting in overestimations
143 (Hendricks et al., 2018a, b; Shi et al., 2021; Wang et al., 2022).
144 For the satellite product, SIA is calculated by multiplying the SIC with the corresponding grid cell
145 area, both derived from the reanalysis dataset provided by the National Snow and Ice Data Center
146 (NSIDC; Comiso, 2017) for the period 2002-2014. SIV is then computed by multiplying the
147 resulting SIA with the satellite-derived floe thickness and summing over the entire Southern
148 Hemisphere.
149

150 *SIT from Reanalysis/Synthesis products:*

151 Reanalyses integrate information from observations and ocean-sea-ice models through data
152 assimilation and provide gridded sea-ice data with homogeneous spatiotemporal sampling over an
153 extended time-period. The use of ocean–sea-ice models forced by atmospheric reanalysis is a
154 general approach to better constrain SIT changes with the observations, in both the Arctic and
155 Antarctic. Since the reanalysis datasets offer state estimations closer to observations compared to
156 model-only data, it makes them a valuable tool in Antarctic sea-ice studies (Kumar et al., 2017).
157 Hence, our study uses two such estimates of long-term Antarctic SIT changes and compares them
158 against the satellite products and the GCMs.

159 GECCO3 ocean synthesis is an improved version of GECCO2 based on MITgcm which employs
160 the adjoint method to fit the model to a large variety of data over a multidecadal period (1948-
161 2018). Unlike GECCO2, it is optimized over only one assimilation window. GECCO3 has 40
162 levels and uses the horizontal and vertical grid of the ocean component of MPI-ESM in the MR/HR
163 configuration, providing a global eddy-permitting synthesis at a nominal resolution of 0.4° (Köhl,
164 2020). While GECCO3 does not directly assimilate sea-ice data, its ocean-ice coupling is
165 influenced by the model's oceanic state. Hence, this synthesis primarily assimilates oceanic data,
166 including temperature and salinity (EN4.2.1), along-track sea-level anomalies (AVISO), and sea
167 surface temperature (HadISST), using a 4D-VAR (adjoint) method (Köhl, 2020).

168 GIOMAS uses the Parallel Ocean Model coupled with a 12-category thickness and enthalpy
169 distribution ice model at a horizontal resolution of 0.8° (Zhang & Rothrock, 2003). In GIOMAS,
170 the modeled SIC is nudged by assimilating satellite-derived SIC from the Special Sensor
171 Microwave Imager (SSM/I) launched by the Defense Meteorological Satellite Program (Weaver
172 et al., 1987). Subsequently, other modeled variables including SIT are adjusted accordingly. This
173 process reduces the root-mean-square difference and improves the correlation between modeled
174 SIT and observed SIT, while also causing the thinning of the mean SIT. This assimilation method
175 has demonstrated good agreement of modeled SIT with satellite observations in the Arctic
176 (Lindsay & Zhang 2006) and is useful for studying long-term variations in Antarctic sea-ice (Liao
177 et al., 2022; Shi et al., 2021).

178 To make the GECCO3 and GIOMAS products comparable to absolute floe thickness estimates
179 (the SIV per grid-cell area or "equivalent sea-ice thickness"), we convert them into "effective
180 thicknesses" by dividing them by their respective SIC records. For the reanalysis/synthesis datasets,
181 SIA is calculated as the product of the SIC and the corresponding grid cell area obtained from the

182 respective datasets. The SIA value so obtained is then multiplied with the "effective thickness" from
183 each of the reanalysis/synthesis dataset to obtain their respective SIV.

184 **2.2 CMIP6 Models**

185 We analyze the *historical* experiments of the CMIP6 dataset, specifically focusing on the *sithick*
186 variable, which represents simulated effective or actual floe thickness. We also use *siconc* (sea-ice
187 concentration) and *areacello* (area of individual grid cells over the ocean) variables. CMIP6
188 models generate multiple ensemble members, which are multiple runs or simulations with slightly
189 different initial conditions or parameter settings, used to capture uncertainty and variability in
190 model predictions. In this study, we consider a single ensemble for each model (Table S2) to
191 account for internal variability and ensure fairness by not giving weight to the models with multiple
192 ensemble members (following Notz & Community, 2020; Roach et al., 2020). We calculate SIV
193 by multiplying *siconc*, *sithick* and *areacello* and summing over the circum-Antarctic Southern
194 Ocean. For SIA, we calculate the area integral product of *siconc* and *areacello*. Lastly, for floe
195 thickness, we use the averaged *sithick* over the Southern Ocean. The multi-model means (MMM)
196 are calculated based on the single ensemble member in 39 coupled climate models for all the three
197 sea-ice variables. In addition to the *historical* experiments, we also analyze a warmer scenario, *SSP*
198 *5-8.5* (Shared Socio-economic Pathway; 2015-2100) to compare with the future sea-ice variability.
199

200 **3. Results**

201 **3.1 Mean and Anomaly State**

202 This section first discusses the mean annual cycles of SIA, SIV and SIT for the different sea-ice
203 products and the CMIP6 models over the period of 2002-2014 (Fig.1). It then examines the biases
204 and spreads in the climate models and, finally, the simulated and observed seasonal trends in the
205 anomalies across all the sea-ice variables.

206 Fig.1a highlights that all the sea-ice products agree on the timing of their SIA maxima and minima
207 (in September and February, respectively). However, GIOMAS, despite having the same
208 maximum and minimum timings, exhibits a lower amplitude, particularly during the winter season.
209 All the CMIP6 models similarly simulate the observed timing of maxima and minima in SIA,
210 however the MMM remains consistently lower than all other sea-ice products throughout the year.
211 Overall, significant negative biases are observed in the simulated SIA cycles, except for a few
212 models that consistently simulate larger SIAs throughout the year.

213 For the SIV, all the sea-ice products display pronounced annual cycles (Fig.1b). While their
214 minima are similar in timing and magnitude, their maxima do not occur at the same time, with the
215 satellite products showing the earliest maxima and GECCO3 the latest. Additionally, the
216 amplitudes of the SIV cycles are highest in the satellite products and lowest in GECCO3. All the
217 CMIP6 models simulate a similar annual cycle to the sea-ice products, with their MMM maxima
218 in October and minima in March (lagging the sea-ice products by one month). Like SIA, the MMM
219 SIV is biased low compared to all the sea-ice products, agreeing best with GECCO3.
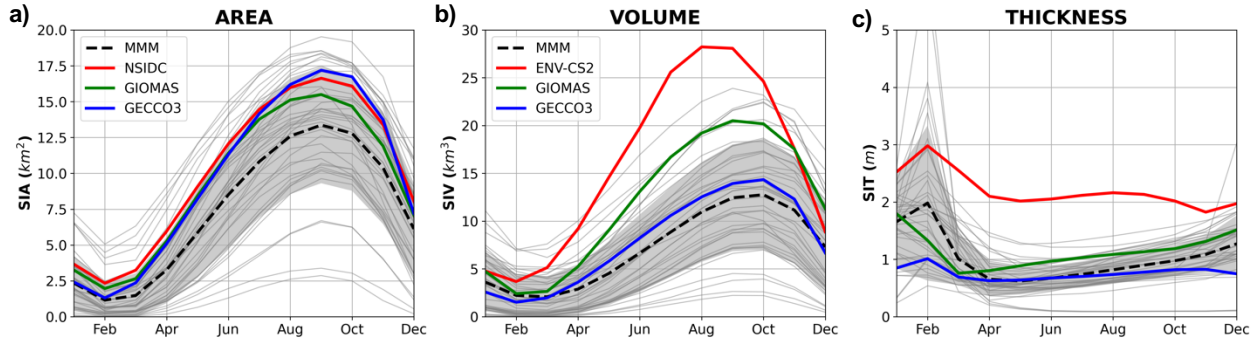
220

Figure 1: Comparison of annual cycles of SIV, SIT and SIA of the circumpolar Antarctic. All the CMIP6 models are shown as grey lines, The Multi-Model Mean (MMM) is the black dashed line. GECCO3 in blue, GIOMASS in green, and Envisat-CryoSat-2/NSIDC in red. Grey shaded areas are +-1 standard deviation for the MMM. Scale: million km² and thousand km³.

Fig.1c shows that SIT has a different annual cycle than SIA and SIV. Its maximum occurs in February, which is observed across all the sea-ice products, except for GIOMAS, where the sea-ice maximum occurs one month earlier. The timing of the SIT minimum is more variable. For the synthesis products, the SIT minimum occurs at the beginning of the growth season, whereas for the satellite products it occurs during the retreating season. CMIP6 models can capture the thickness maxima in February and agree with the synthesis products in showing minima in the fall. However, there is considerable spread in the exact timing of the minimum, with the MMM minimum occurring in May, lagging the reanalysis products. Most of the models simulate thicker sea-ice than the three sea-ice products during summer (between January-April) resulting in biases which considerably decrease for the synthesis products and increase for satellite datasets starting in May. A few models, namely the IPSL and EC-Earth3-models (characterized by significant warm Southern Ocean biases; Döscher et al., 2022), exhibit anomalously thick sea-ice (>3m) in February. This can be attributed to the dynamically-related reasons causing the drift and deformation of the ice. This thick ice is captured in these models mainly due to the well-resolved wind patterns (Vancoppenolle et al., 2009) which result in the sea-ice drift and accumulation of the multi-year ice which survives the summer melt and is found mainly in the Weddell Sector during February. Additionally, in models with NEMO-LIM3 sea-ice modules, such as IPSL- and the EC-Earth3-models, the frazil ice formation dominates the total ice growth which may again lead to an accumulated SIT during February (Lie et al., 2021). By contrast, CNRM-models exhibit anomalously low thickness throughout the year. This is primarily due to high negative biases in their SIC simulations and their inability to realistically simulate thick sea-ice during the austral summer in the Weddell Sea (Voldoire et al., 2019). Moreover, these differences can be attributed to various factors, including the multiyear sea-ice surviving the summer melt (Worby et al., 2008), challenges associated with satellite retrieval of summer SIT (Kurtz and Markus, 2012), and the influence of dynamical wind patterns in CMIP6 models, resulting in excessive ridging (Lie et al., 2021).

Summer maxima in SIT vary between January and February depending on the sea-ice product used (Fig.1c). Such high SIT values during summer stand in contrast with the annual minima observed in other sea-ice variables. This SIT annual cycle results from the melt of first year ice in large areas in the seasonal ice zone so that only the thickest ice survives. In the beginning of the freezing

258   season, large areas are covered by newly formed first year ice, which reduces the mean freeboard
259   compared to summer values (Schwegmann et al., 2016). Therefore, the highest average thickness
260   in February is due to the compacted ice which survives the melt season (Kurtz & Markus, 2012;
261   Worby et al., 2008; Xu et al., 2021). It is for this reason that the SIT seasonal cycles look very
262   different from those of SIA or SIV. Therefore, to capture the sea-ice seasons based exclusively on
263   the annual cycle of SIT, we conducted the analyses in Sect. 3.3 and 3.4 using February and
264   September.

265   The inter-model agreement also varies considerably between seasons and across variables. The
266   inter-model spread of annual mean Antarctic SIT, SIV and SIA is 5.9 m, 20 thousand km^3 and 16
267   million km^2 for the maxima and 1.8 m, 7.5 thousand km^3 and 4 million km^2 for the minima,
268   respectively. Fluctuations in the inter-model spread are larger during fall and winter for SIV and
269   SIA but shrinks during summers. By contrast, SIT has greater inter-model spread during summer
270   and shrinks significantly from April-November. Notably, for most parts of the year, the inter-
271   model spread in SIT remains smaller than disagreements within the sea-ice products, owing to the
272   overestimations in satellite product during the winter months.
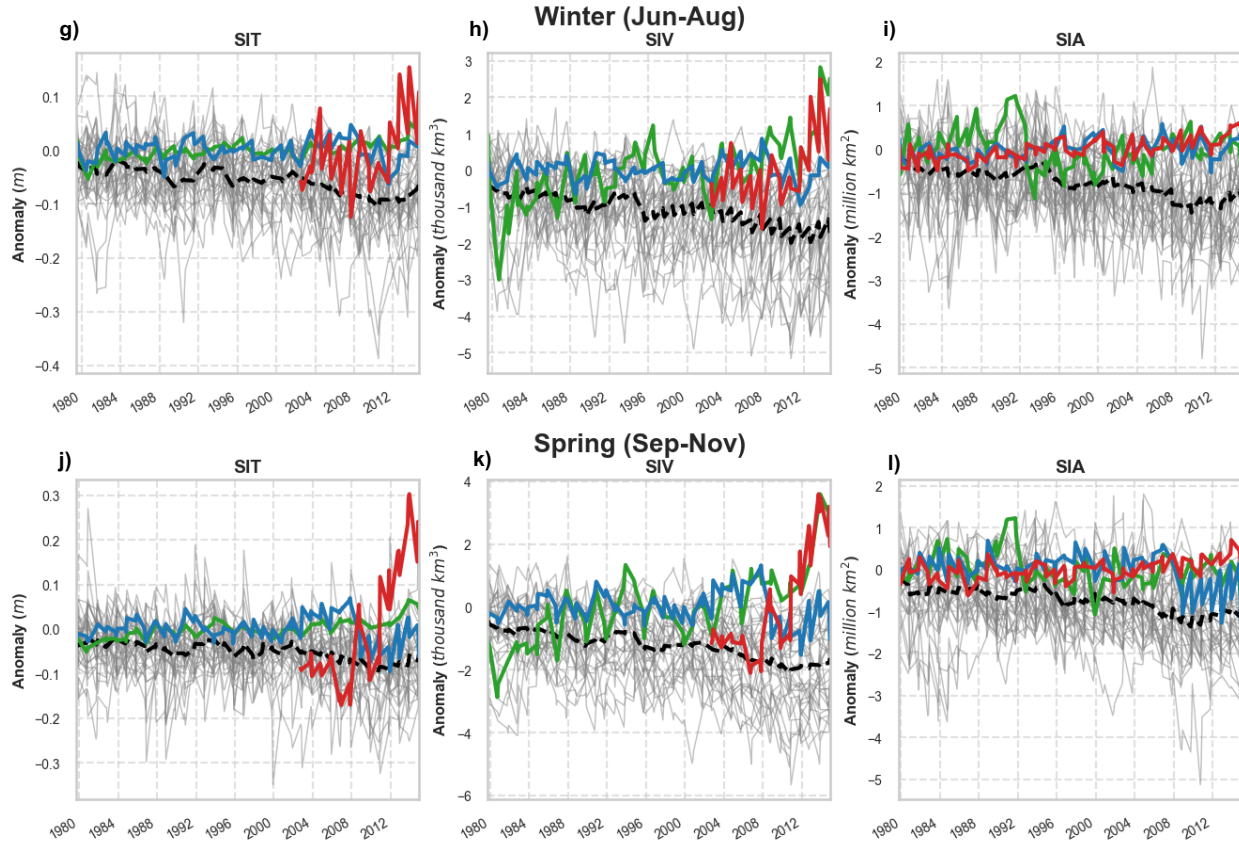
273

274

275

276
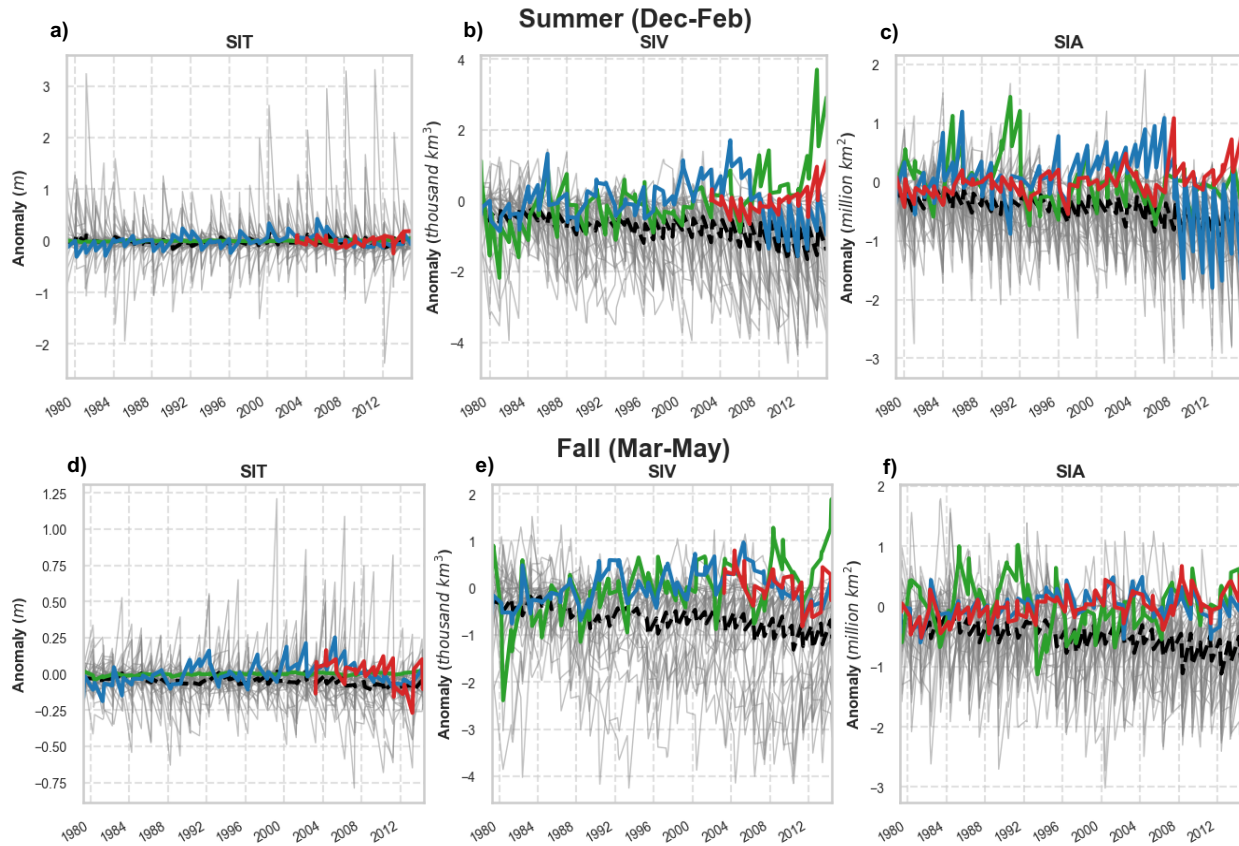
Figure 2: Anomalies for four seasons: Summer and Fall (Warm Seasons; a-f), Winter and Spring (Cold Seasons; g-l) of SIT (left), SIV (middle) and SIA (right) of the circumpolar Antarctic. All the CMIP6 models are shown as grey lines, Multi-model mean in dashed line, GECCO3 in blue, GIOMASS in green, and NSIDC/ Envisat-CS-2 in red. All the sea-ice products extend for the time-period 1979-2014 except for satellite products which are only available for 2002-2014.

Next, we look at the seasonal trends in the anomalies of the three sea-ice variables (SIT, SIV and SIA) across different CMIP6 models and the sea-ice products. In general, CMIP6 models simulate negative trends in Antarctic SIA and extent (Roach et al., 2020 and Shu et al., 2020), which contrast with the observed positive trend until mid-2015 (Li et al., 2023; Shu et al., 2015; Turner et al., 2013). Figure 2 demonstrates a similar pattern in the simulated SIT/SIV with a negative trend noticed across all the sea-ice variables. However, differences emerge in seasonal trends for different sea-ice products (blue lines for GECCO3; green for GIOMAS and red for the satellite products in Fig.2) starting in the early 2000s.

In particular, significant positive trends in SIT/SIV are observed during the cooler seasons (winter and spring; Fig.2g-h,j-k), while no such trends (or very weak trends in SIV) are detected in the warmer seasons (Fig.2a-b,d-e). For SIA, small positive trends are observed during the warmer seasons (Summer and Fall), consistent with the previous studies (Martinson, 2012; Eayrs et al., 2019), while these trends are markedly reduced during the cooler seasons. This reduction is attributed to the thermodynamic constraints imposed by the Southern Ocean polar front, which limits ice edge expansion during the colder months. The observed positive trends in SIT/SIV during winter and spring imply that changes in Antarctic SIT may contribute to variability in total

9

299 sea-ice mass/volume during these colder months. This could be linked to the presence of robust
300 land-ocean temperature gradients during winters, which may result in high-intensity winds, one of
301 the significant contributors to SIT/SIV fluctuations in the Southern Ocean (Zhang, 2014).

3.2 Future Projections under *SSP5-8.5 (2015–2100)*

303 Since our study uses *historical* experiments in climate models which ends in 2014 (due to the cut-
304 off limits of the *historical* simulations), this section acknowledges the importance of assessing
305 future sea-ice developments, particularly in the Antarctic where pronounced declines in the sea-
306 ice have been observed since 2016 (Eayrs et al., 2021; Raphael and Handcock, 2022; Wang et al.,
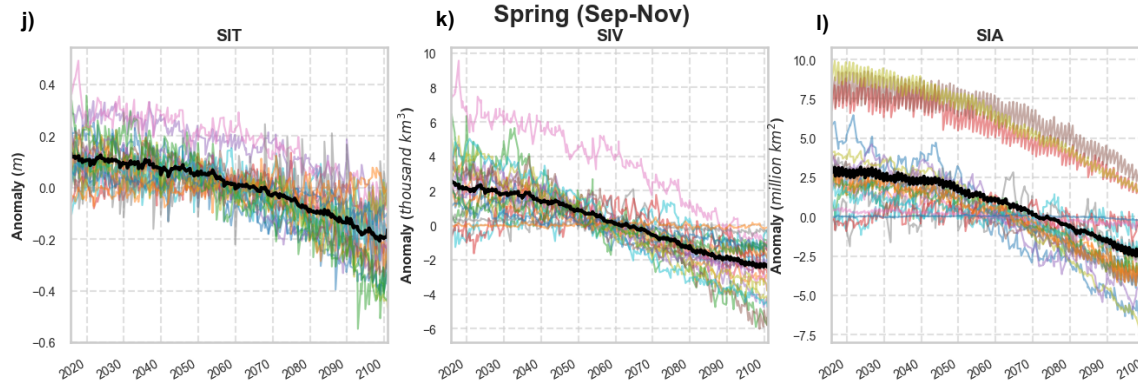307 2022; Turner et al., 2022).
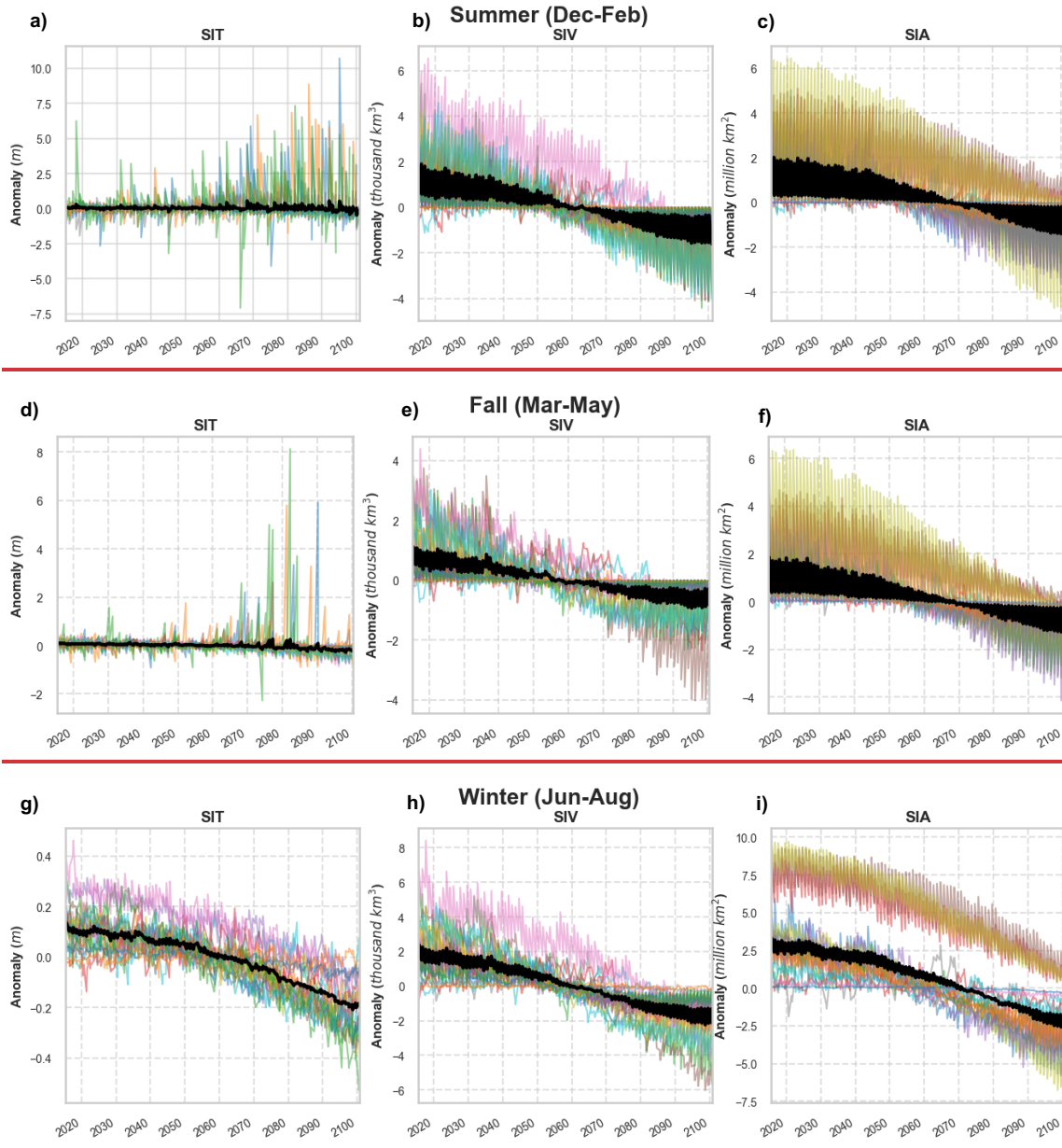
Figure 3: Anomalies for four seasons: Summer and Fall (a-f; Warm Seasons), Winter and Spring (g-l; Cold Seasons) of SIT (left), SIV (middle) and SIA (right) of the circum-Antarctic. All the CMIP6 models are shown as colored lines, and the Multi-model Mean in black line. The time-period is 2015-2100 for the *SSP5-8.5* scenario. Since sea ice products end in 2014, they could not be included here. Note that 3 models (namely ACCESS-CM-2, ACCESS-EM2-1 and CESM2-WACCM show slightly higher anomalies (especially for SIA), particularly evident during the cooler seasons (i and l).

~~Therefore, w~~We examined the seasonal anomalies in sea-ice variables under the high-emission *SSP5-8.5* scenario for the period 2015–2100 (Fig. 3). The results are consistent with those in Fig. 2, showing pronounced seasonal trends in SIT, particularly during the cooler seasons (winter and spring). Under the warmer scenario, all CMIP6 models project a notable decline in SIT during these cooler months, while trends in SIT are largely absent during the warmer seasons (summer and fall). In contrast, SIV and SIA exhibit a persistent year-round decline, with negative anomalies becoming more pronounced from approximately 2060 onward (Fig. 3).

When assessing the Antarctic sea ice distributions in the post-2014 period, it is expected that under warming scenarios, models will show reductions in sea ice owing to their response to increasing temperatures. However, our results reveal a seasonally asymmetric pattern of decline: SIA and SIV decrease persistently throughout the year, while SIT exhibits notable thinning only during cooler seasons. This indicates that the overall reduction in Antarctic sea ice projected under warmer scenarios is likely driven by sustained losses in area and volume as actual thinning is not consistently observed across all seasons. Consequently, much of the reduction in simulated sea ice likely arises from changes in surface coverage rather than from widespread structural thinning. These projected declines also correspond well with the observed post-2016 record-low Antarctic sea-ice extents (Turner et al., 2017; Schlosser et al., 2018), indicating that the recent losses may represent the early onset of the long-term downward trend simulated under high-emission scenarios. Such consistency between observations and projections highlights the increasing vulnerability of the Antarctic sea ice system to ongoing atmospheric and oceanic warming. Future studies are needed to investigate this in detail.

3.3 Seasonal Variations and Inter-relationships

11

343   An accurate spatio-temporal distribution of SIT is key to accurate estimates of SIA and eventually
344   SIV distributions. It reflects the skill in simulation of local processes, coupled interactions and
345   energy transfer among the ocean below, the sea-ice, and the atmosphere above (Stroeve et al.,
346   2014). To estimate seasonal variations and evaluate the performance of the CMIP6 models in
347   capturing the observed distribution of sea-ice variables, we plot the Taylor Diagrams (Fig.4)
348   representing the spatial correlation coefficients, Root Mean Square Deviation (RMSD; not shown
349   in the Figure but included in Tables S3-S5) and standard deviation among 39 models, and the three
350   sea-ice products. We use the satellite dataset as the observation reference for SIT and SIV,
351   calculating RMSDs and correlation values across the grids. For SIA, the reference dataset used is
352   NSIDC. All the calculations were performed based on area-integrated spatial averages of reference
353   datasets of SIT, SIV and SIA over the circum-Antarctic for February and September.
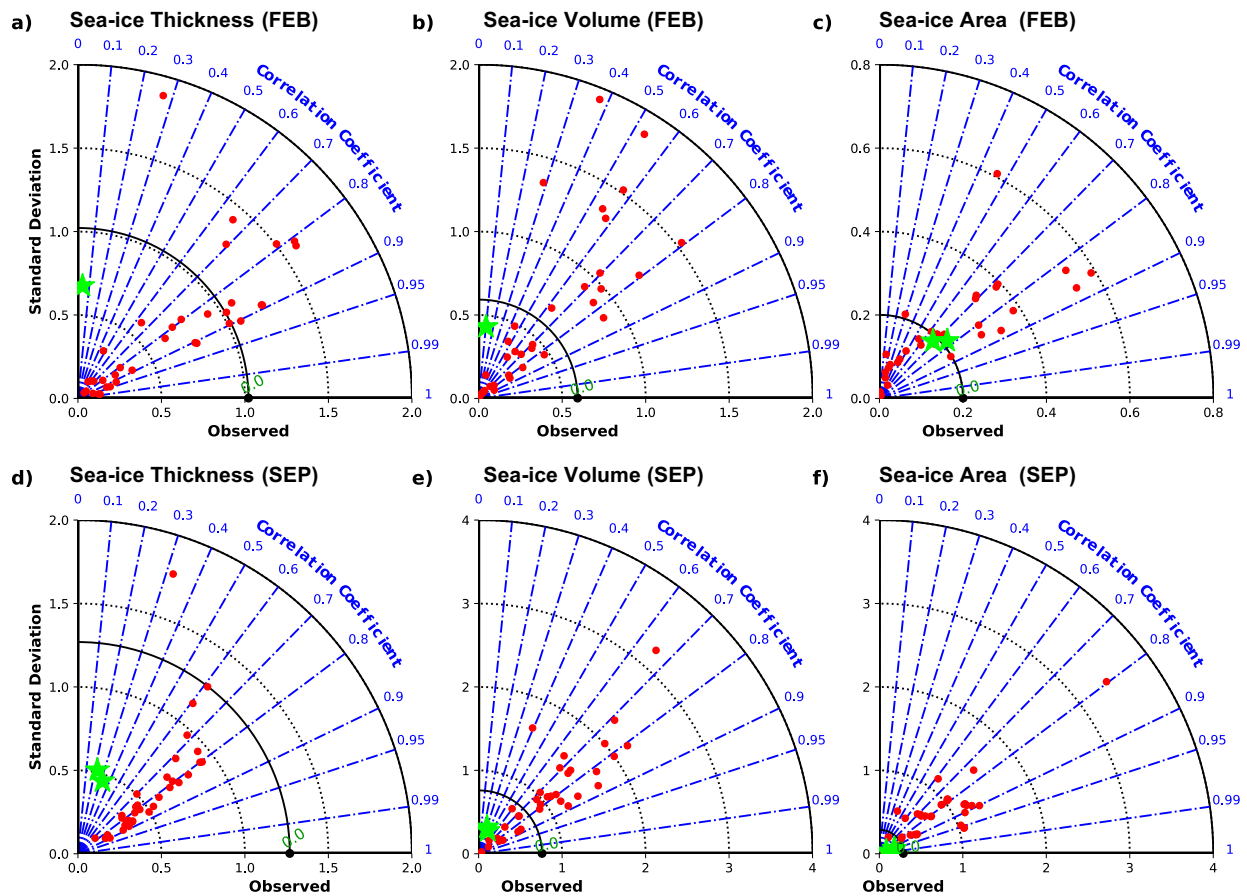
354

355

356

**Figure 4: Taylor Diagrams representing spatial correlation and standard deviation using
time-averaged means between CMIP6 models and different sea-ice products. For each
model and synthesis product, two statistics are plotted: the Pearson correlation coefficient,
related to the azimuthal angle (blue contours); and the standard deviation viz proportional
to the radial distance from the origin (black dotted contours). Black solid contour
corresponds to the standard deviation of the reference dataset. Red dots represent
individual CMIP6 models and green stars represent synthesis datasets. The period used for
comparison is 2002-2014 for February (a,b,c) and September (d,e,f). For February (a and
b), GECCO3 is not included as it had very small negative correlation coefficients.**

366 **Reference datasets used for SIT/SIV and SIA are Envisat-CryoSat-2 and NSIDC,**
367 **respectively. Higher correlation coupled with a lower RMSD indicates greater accuracy of**
368 **CMIP6 models in simulating the sea-ice variables.**

369 The correlation coefficients in Fig.4 range between 0.6-0.9 for all the variables in both the months
370 (Tables S3, S4 and S5). Specifically, models tend to exhibit the highest variability in SIT, as
371 indicated by higher RMSDs and standard deviation values that deviate significantly from those of
372 the reference dataset (Fig.4a,d). Both synthesis products (GIOMAS and GECCO3) show the
373 highest variability and lowest correlations for SIT, indicating lack of agreement among different
374 sea-ice products. Whereas the opposite is observed for SIA where most of the models and
375 reanalysis products have a lower variability for SIA (Fig.4c,f) compared to SIV and SIT. When
376 comparing the two months, lower variability and higher correlations are observed for all the sea-
377 ice variables in February (Fig.4a-c). In summary, the Taylor Diagram reveals that while most
378 CMIP6 models demonstrate higher accuracy in simulating SIA and SIV (with high correlations
379 and low RMSDs), their SIT simulations are less accurate. The widely spread standard deviations
380 suggest considerable differences in how the models simulate internal variability in SIT,
381 highlighting their underlying uncertainties in representing such variability. There also exists a
382 disparity in their seasonal accuracy with models performing better during February across all the
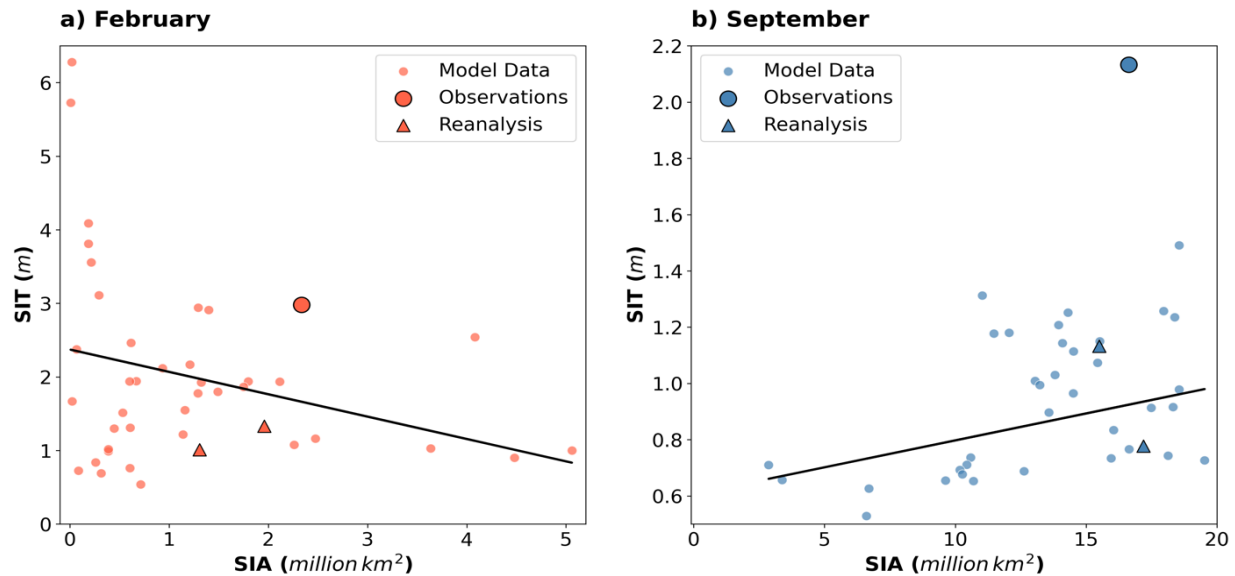383 variables.

384
385 **Figure 5: Scatter plots between the climatological means of SIT (y-axis) and SIA (x-axis)**
386 **for CMIP6 models and Observations for the period (2002-2014) for February (red) and**
387 **September (blue). The line of best fit represents the relationship between the two variables**
388 **for selected months. Each small dot represents a model while the larger dots represent**
389 **observations (Envisat-CryoSat-2 and NSIDC for SIT and SIA, respectively). The**
390 **reanalysis/synthesis datasets are represented by triangles. The figure clearly demonstrates**
391 **seasonal variations in magnitudes of both the variables.**

392 Given their better performance in simulating SIA, we further investigate whether or not this
393 performance is correlated with SIT accuracy in individual CMIP6 models and the synthesis
394 products. This evaluation has not been done before; however, examining this interrelationship will
395 significantly enhance our understanding of sea-ice changes, which has so far been largely based

396 on surface parameters such as SIA. Additionally, it will provide deeper insights into the
397 interpretation of existing historical records of surface sea-ice parameters in the Antarctic. For this,
398 we compare the annual averages of SIT and SIA in models and the synthesis products using the
399 satellite product as the observational reference (Fig.5). The comparison shows that SIA biases range
400 between -2 to 2 million km^2 during February and between -14 to 4 million km^2 during September.
401 In February, although SIT is at maximum, most models simulate thinner sea-ice with values below
402 the satellite estimates of 3m. During September, the models consistently show thin biases with
403 values ranging between 1-2m across all the models.

404 Figure 5 also highlights how simulated SIA and SIT are differently related depending on the time
405 of year (also evident in Fig.2-3). In summer, SIA and SIT biases are negatively correlated (Fig.5a;
406 although we note that many models have very low SIA in February), and in winter they are
407 positively correlated (Fig.5b). One possible way to explain this is that models with strong melt
408 seasons result in low summer sea-ice cover in which only the thickest ice can survive. The reverse
409 may be true for weaker melt seasons which may allow more, and thinner, ice to survive, leading
410 to greater SIA made up of thinner ice. In winter, greater sea-ice freezing will lead to both thicker
411 ice and a larger area, explaining the positive relationship between the SIA and SIT biases in Fig.5b.
412 This contrasting seasonal relationship raises questions about whether SIA is a reliable predictor of
413 SIT, which has significant implications for our understanding of sea-ice changes when based solely
414 on SIA. Further studies are needed to clarify this.

3.4 Seasonality in SIT Biases

416 This section investigates the seasonality in SIT biases in both temporal and spatial dimensions
417 across three sea-ice products, relative to the multi-model means (MMM) of the selected 39 CMIP6
418 models. Figure 6 highlights the seasonality in SIT biases, showing patterns in biases with reference
419 to the climatological SIT means across different months and sea-ice products. With respect to the
420 satellite product, most models exhibit negative biases across all months, with the largest bias
421 observed in March. For the two reanalysis/synthesis datasets, the simulated SIT MMM values,
422 except for the February maxima, remain closer to the zero line (within the range of ±0.3m),
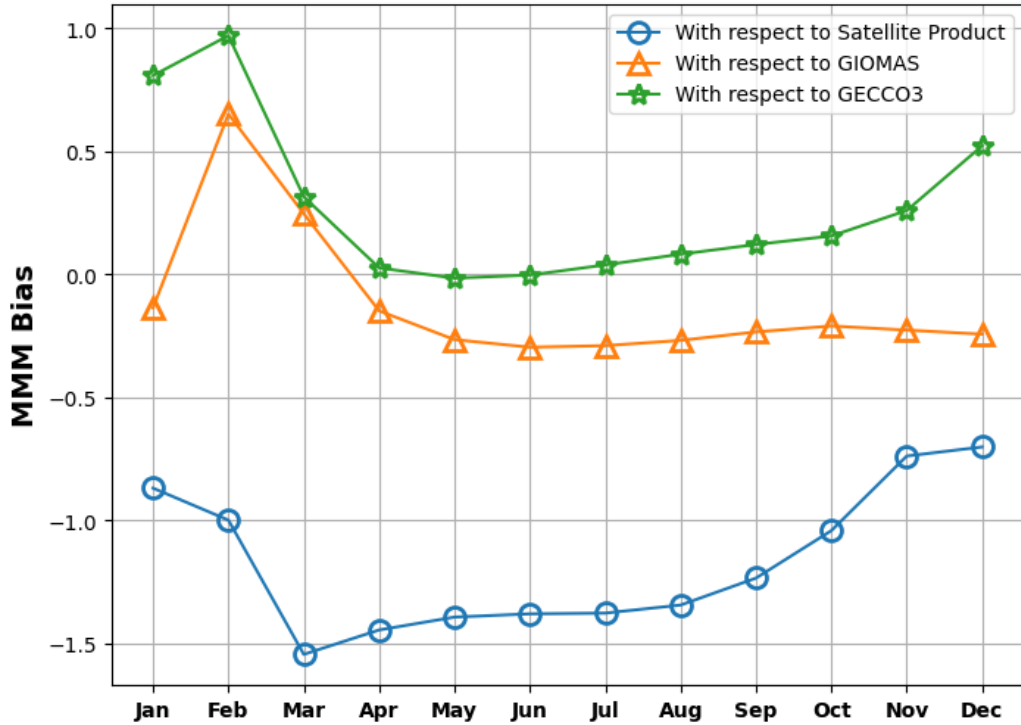423 indicating much smaller biases.

Figure 6: Seasonality in SIT biases (m) calculated as the difference between climatological means of MMM of 39 CMIP6 models and the three sea-ice products (2002-2014).

This section further explores the spatial spread (measured by the standard deviation of the ensemble) in SIT and SIC biases, using three different sea-ice products for February (Fig.7) and September (Fig.8) over the period 2002-2014. In February, higher standard deviations are evident in the Amundsen-Bellingshausen Seas (ABS) and along the coastal edges of the Weddell Sea (blue shaded regions in Fig.7a), indicating greater model disagreement when compared to the sea-ice products during this month. These regional disagreements may result from dynamic processes such as sea-ice drift, melting, and freezing which are not accurately captured by the models. However, models generally show better alignment with reanalysis/synthesis products in February, as seen in the lower standard deviation values (shown in red), indicating improved agreement.
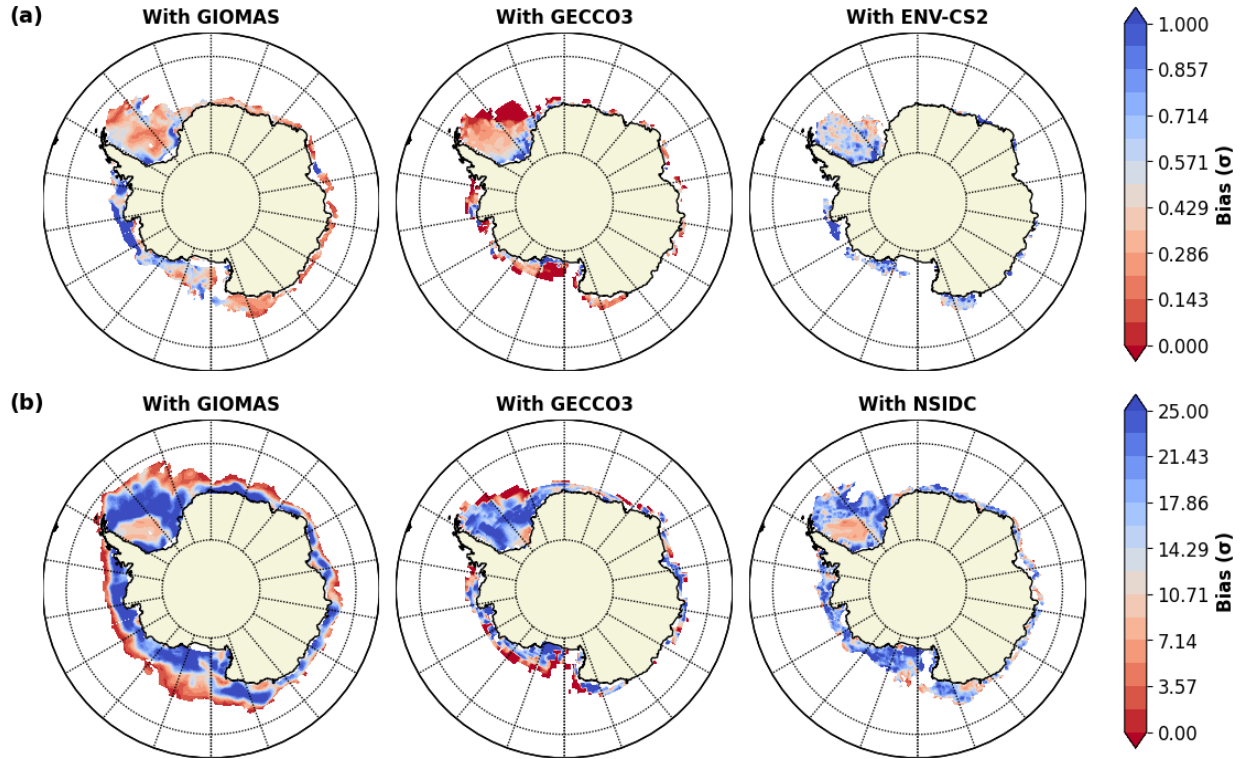
Figure 7: Variability of the Spatial Biases in CMIP6 Models (calculated as Standard Deviation of the difference between CMIP6 MMM and the three distinct sea ice products); for the month of February in (a) SIT (m) and (b) SIC (%).

In contrast to SIT, the spatial bias spread in SIC is larger (Fig.7b), but the pattern remains similar— better model agreement (lower standard deviations) at the ice edges and in the inner Weddell Sea, while there exists poorer agreement (higher standard deviations) closer to the coasts. Figure 7b also helps to determine how SIC biases may contribute to standard deviations observed in the SIT biases. For instance, the regions of higher model disagreements in SIT that coincide with the high SIC standard deviations suggest that model errors in locating the ice edge may also influence the spread of actual thickness and vice versa. Therefore, when models misplace the ice edge, they might overestimate or underestimate SIT in those regions. In February, the model disagreements in the SIT biases near the ABS and the coastal edges of the Weddell (blue regions in Fig.7a) coincide with higher standard deviation values in SIC bias spread (Fig.7b) in the same regions, especially along the southern Weddell coast. This suggests that some of the SIT biases in these regions could be a result of misrepresentation of the ice edge in models, rather than true variations in actual thickness.

In September, there is an overall lower bias spread in SIT across most of the Antarctic region, except for localized areas along the sea-ice edge where model disagreement is more pronounced, particularly in the ABS and the Eastern Antarctic, and the coastal edges of the Weddell Sea along the Antarctic Peninsula (Fig.8a). When comparing across all the sea-ice products, a relatively higher standard deviation value is noticed in most of the Antarctic regions with respect to the satellite product (Fig.8a). This can be attributed to the satellite product's exaggerated SIT values for September which most models are unable to simulate, leading to greater model disagreements.
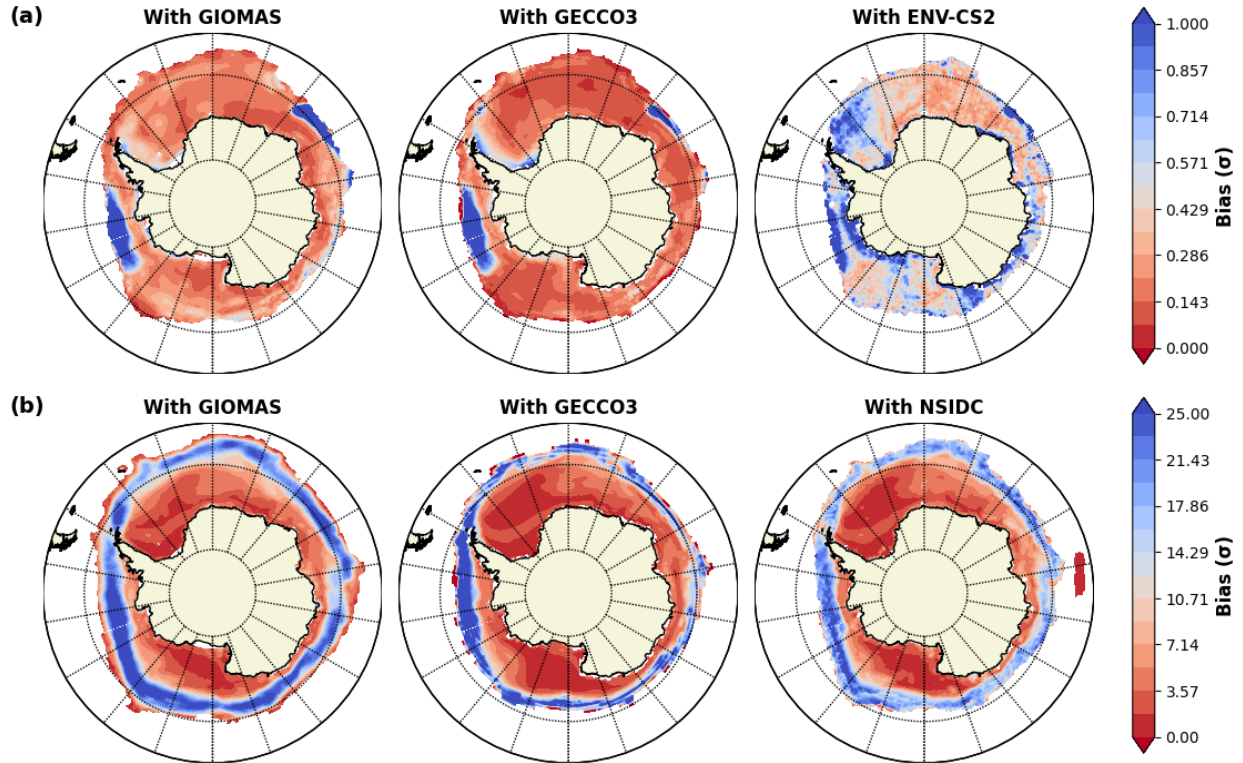
Figure 8: Variability of the Spatial Biases in CMIP6 Models (calculated as Standard Deviation of the difference between CMIP6 MMM and the three distinct sea ice products); for the month of September in (a) SIT (m) and (b) SIC (%).

Figure 8b shows SIC bias spreads for September, where much of the Antarctic region displays low standard deviation values. However, the sea-ice edge remains an area of higher model disagreement, similar to the SIT patterns, suggesting that while the ice interior is well-represented, models continue to struggle with accurately locating the ice edge. The correlation between SIC and SIT bias spreads is again observed in September, where model disagreements along localized ice edges occur in both variables, indicating that SIT biases in CMIP6 models may stem, in part, from uncertainties in where the ice edge is located. However, along the coastal edges of the Antarctic Peninsula, the lower SIC standard deviation values compared to that of SIT suggest that the model disagreements in SIT are more likely driven by the differences in how models simulate dynamic processes (e.g., the Weddell gyre and its role in sea-ice dynamics) rather than by inaccuracies in the ice edge representation. The following section addresses this in more detail across individual models.

3.5 Spatial Distributions of SIT

In this section, we perform a spatial comparison for circum-Antarctic SIT across 39 individual CMIP6 model ensembles using different sea-ice products as observational references. However, we only discuss in detail GIOMAS as the observational reference. Here, GIOMAS is selected for a detailed discussion instead of other sea-ice products, primarily due to its relative overall closer agreement with the models (See Sec.3.1) and the very high SIT biases observed in the satellite

488 products during September (Fig.6 and S1). In general, during both the months the mean spatial
489 distribution of SIT in models shows lower biases with respect to the reanalyses/syntheses when
490 compared to the satellite product (See Sect.3.4). GECCO3 produced results comparable to the
491 GIOMAS reanalysis product (not shown). Although GIOMAS displays an earlier seasonal
492 maximum, the MMMs exhibit the lowest biases relative to GIOMAS for this month, compared to
493 GECCO3 and satellite-derived products (Fig.6).

494 Spatially, the satellite as well as the reanalysis/synthesis products show that thickest sea-ice resides
495 in the western Weddell Sea along the Antarctic Peninsula and along the coastal edges of the ABS-
496 in the form of multi-year ice (Fig.9 and S1). There is relatively thinner sea-ice observed in the
497 eastern Antarctic (Kurtz & Markus, 2012). Our analysis reveals that most of the CMIP6 models
498 capture a similar spatial pattern in SIT around the Antarctic however, they do exhibit biases and
499 underestimate SIT (Fig.9 and Fig.S1-S3). In February, over half of the models simulate thinner
500 sea ice in the Weddell Sea compared to the GIOMAS product (Fig.S2) while thin biases relative
501 to the satellite products are simulated almost across all the models (Fig.S3). On the circum-
502 Antarctica scale, about 38% of the models simulate thicker ice compared to GIOMAS, with only
503 5 out of 39 models showing SIT greater than that estimated by satellite products.

504
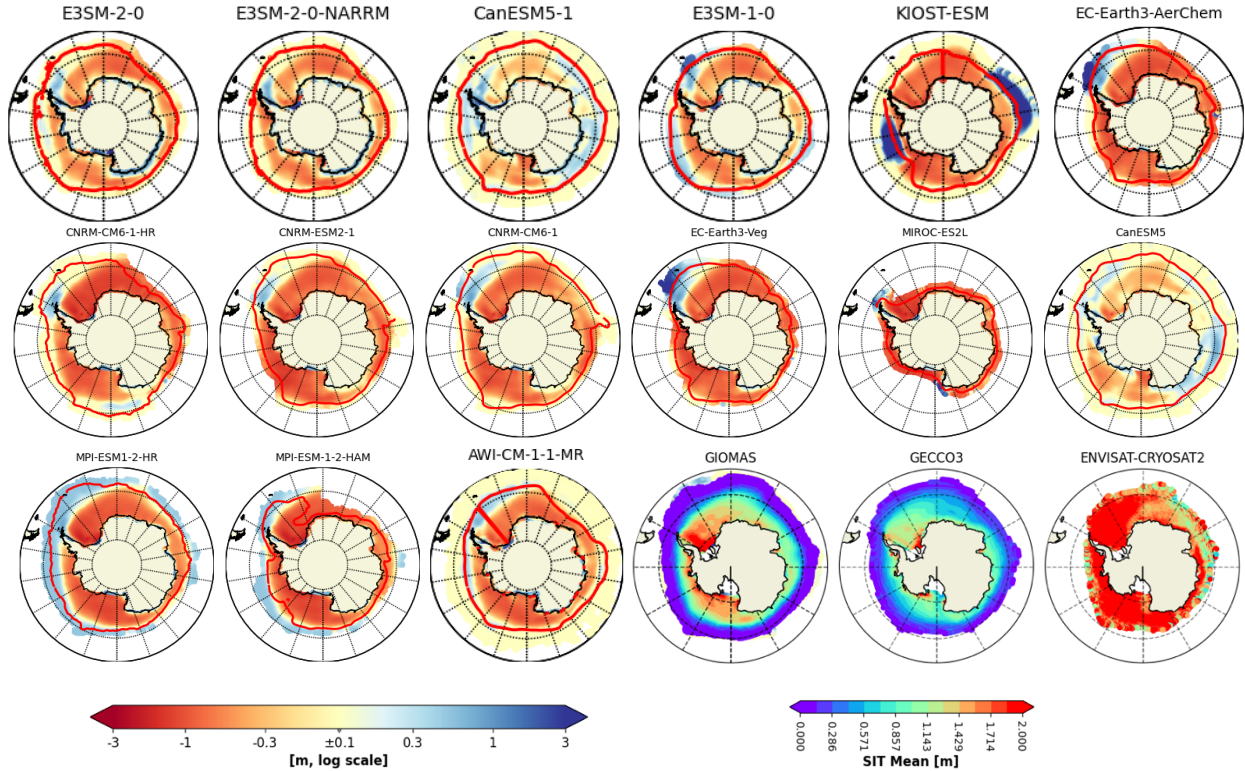

508

509

510

511
512

513
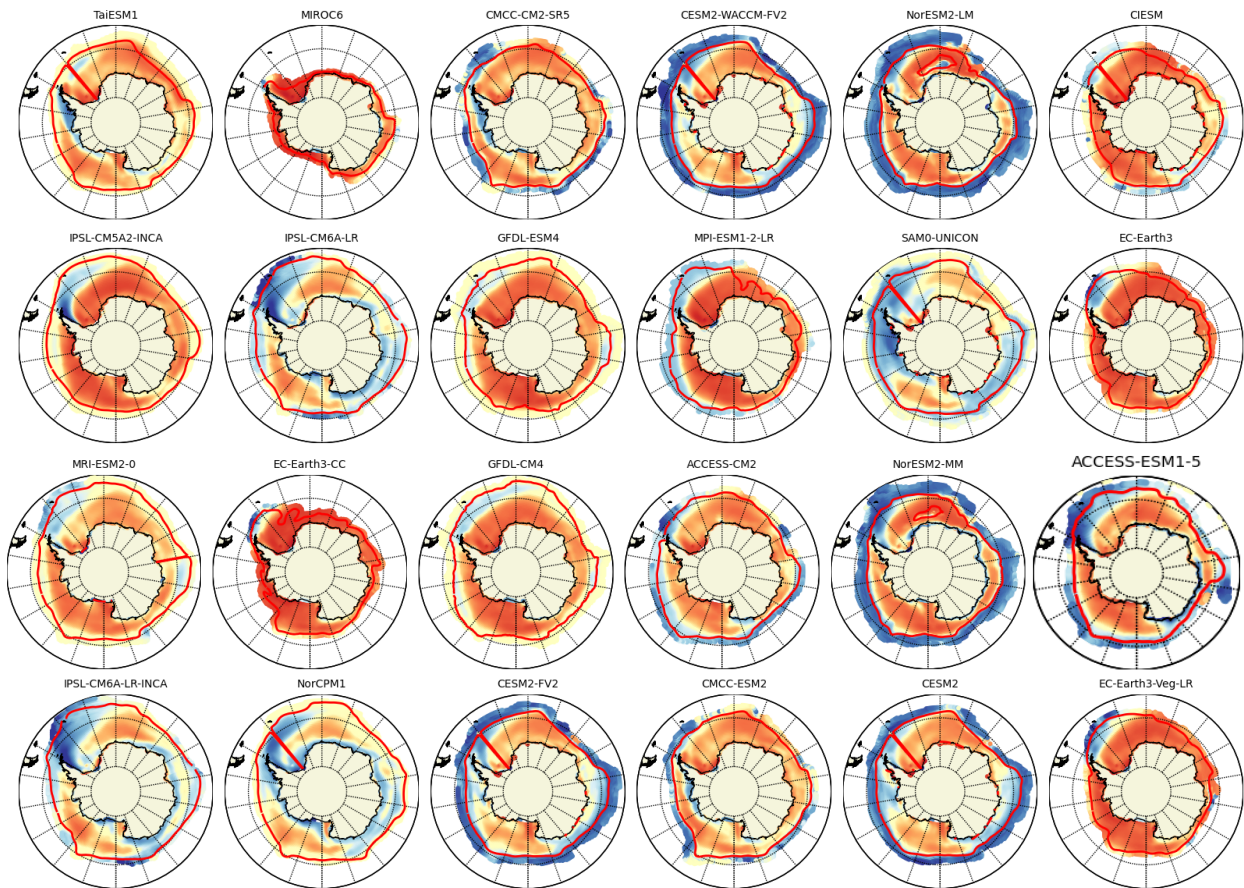
Figure 9: Spatial Biases of SIT averaged over 2002 to 2014 (September) for 39 CMIP6 models from the reference dataset: GIOMAS. The last three plots show the time averaged SIT for the three sea-ice products. The red contours represent the sea-ice edge.

The spatial patterns of SIT in September (Fig.9) show anomalously thick ice (>3m) in some CMIP6 models primarily in *two* regions: an elongated *tongue of thickest sea-ice* extending northward from the northwest Weddell Sea along the Antarctic Peninsula and, the other is *around the sea-ice edge*. The distinctive tongue-like pattern may be attributed to a prominent feature in the Weddell Sea called the *Weddell Gyre* (Vernet et al., 2019). This mechanism contributes significantly to the regional sea-ice dynamics in the form of an apparent westward ice motion in the southern Weddell Sea. As a result, ice convergence occurs in the southwestern Weddell, causing dynamic thickening (Shi et al., 2021). Multiple models, including IPSL-CM6A-, EC-Earth3-, NorCPM1, and ACCESS-models, which captured this tongue of thick sea-ice, also effectively captured the Weddell Gyre through their well-developed sea-ice velocity vectors (not shown). This is one of the primary reasons why these models simulate excessively thick ice along the Peninsula (Li et al., 2021). A similar spatial pattern in SIT was also observed using ICESat measurements (Holland & Kwok, 2012) and in simulations from an ocean-sea-ice model in the Southern Ocean (Holland et al., 2014).

The other region of thick sea-ice bias is the *sea-ice edge* (Fig.9). It's interesting to note that the CMIP6 models that have exhibited better performance in simulating Antarctic SIA, such as CESM2-, NorESM2-, and ACCESS-models (Holmes et al., 2019; Li et al., 2023; Roach et al., 2020; Uotila et al., 2014) show positive thickness anomalies/biases all around the sea-ice edge during September, north the 15% SIC interval. A potential explanation for this could be through combinations of changes in air-ice drag and the direction of cold or warm-air advection. These may result in northward wind stress causing the sea-ice to drift, transport and accumulate causing

539 dynamic convergence at the sea-ice edge (Singh et al., 2021; Holland et al., 2014; Holland &
540 Kwok, 2012). Another reason could be the high-intensity ocean-wave fields linked to the Southern
541 Ocean which deeply infiltrate the marginal ice zone. This penetration induces alterations in
542 thickness distribution through processes like rafting and ridging, especially in the vicinity of the
543 ice edge (Langhorne et al., 1998). In any case, the simulated sea-ice at the ice edge is much thicker
544 than observed and further study is required to eliminate modeling error as its cause.

545 Among the CMIP6 models, there are two clear patterns that emerge across the smaller subsets
546 (Fig.9): *First*, a general "thin" bias in the models which is observed throughout the ice pack at all
547 longitudes, coupled with a "thick" bias in the marginal ice zone/ice edge (as seen in CESM2,
548 NorESM2, and ACCESS), likely reflecting the net northward transport of Antarctic sea-ice.
549 *Second*, another smaller subset of models (such as IPSL, SAM0-UNICON, NorCPM1, CESM2,
550 and CanESM5) which exhibit more zonally assymmetric biases, providing distinct signatures of
551 the Ross and Weddell gyres—particularly in the form of thick ice at the outflow and thin ice at the
552 inflow. Both modeled patterns underscore the importance of sea-ice dynamics and invites further
553 investigation.

554 Additionally, Fig.9 and S1-S3 depict varying model spreads in SIT simulations with noticeable
555 differences in their spatial biases and distributions. These variations are largely driven by
556 differences in parameterization schemes and the representation of underlying physical processes
557 across the models. While these discrepancies affect the accuracy of SIT simulations, a detailed
558 examination of each model's parameterization and physics is beyond the scope of this study. Our
559 primary focus is on the broader evaluation of the spatial distribution of SIT across the models and
560 their comparison to observational and synthesis datasets.

561 In summary, all models tend to underestimate SIT and produce relatively thinner sea-ice during
562 both September and February. These negative biases are more pronounced in September and much
563 less pronounced in February. When comparing among the reference products, models simulate
564 SIT closer to the reanalysis reference, i.e. GIOMAS, in both months with about 50% of the CMIP6
565 models (20 out of 39) having their mean spatial biases between +/-0.5m. Notably, one of our
566 comparisons uses satellite products, which exhibit some uncertainties in estimating SIT in the
567 Southern Ocean, particularly showing thicker values in September. Therefore, models displaying
568 even greater positive biases (>1m) in September compared to the satellites (Fig.S1) may be
569 simulating excessively thick sea-ice, potentially presenting a false picture of future Antarctic sea-
570 ice changes.

571

4. Discussion

573 Antarctic sea-ice thickness (SIT) exhibits a seasonal cycle different from other surface sea-ice
574 parameters with its maxima observed in February, when only the thickest multi-year ice survives
575 the melt season. CMIP6 models generally capture this behavior, successfully simulating peak
576 thickness in February. This agreement at summer maxima suggests that model thermodynamics
577 allow a remnant of thick ice to persist through austral summer, similar to observations. During
578 winter growth, however, Antarctic ice remains relatively thin on average. The thickness minimum
579 occurs in late fall or early winter, depending on the type of SIT dataset.

580 Besides the thermodynamic factors, the observed discrepancies in the CMIP6 models with
581 different sea-ice products can be due to a variety of factors such as model parameterizations and

tuning, snow ice interactions or other sea-ice processes. CMIP6 models generally capture the spatial pattern of thicker coastal ice versus thinner ice elsewhere, but they tend to underestimate the absolute thickness in these deformed-ice regions (~58% less than satellite-based estimates; Hou et al., 2024). This bias points to limitations in model dynamics: if ridging schemes or ice strength parameters are not adequately representing pressure ridge formation, models will produce too little thick ice. Moreover, the ice thickness distribution in models is sensitive to mechanical parameters– e.g. the compressive strength and the number of thickness categories –which control how readily ice converges into thick ridges (Nie et al., 2023). Numerical experiments confirm that increasing the number of ice thickness categories or a higher horizontal model resolution improves the simulation of thick ice: more categories allow a better representation of high-thickness tails from ridging and finer grids reduce artificial numerical diffusion of ice thickness.

Model parameter tuning can also impact thickness. Sea-ice models are often tuned to get realistic ice extent or concentration, which can indirectly affect SIT. For instance, adjusting albedo or ice strength to match observed ice area might cause models to grow ice either too thick or too thin as a side effect. Similarly, the GIOMAS reanalysis (with ~0.8° grid and concentration assimilation) is also known to underestimate thickness in deformed ice areas, partly due to smoothing and assimilation removing thick ice (Liao et al., 2022). This underestimation is echoed in many CMIP6 models. Studies of Arctic sea-ice in models have shown that tuning ice strength and improving ice drift physics can reduce biases in ice thickness and extent. In the Antarctic, this means capturing features like the persistent Weddell Gyre (which retains most of the multi-year ice) and properly accounting for wave-induced ice break-up and floe size effects in the outer pack. Improving sea-ice dynamics in models (ridging parameterizations, drag coefficients, and interactions with ocean currents) is essential for simulating the observed thick ice in convergence zones. Model biases in atmosphere or ocean state can also translate into SIT biases, depending on how the sea-ice model is tuned. Therefore, diagnosing thickness biases requires careful attention to model configuration: ice strength parameters, snow thermal conductivity, melt pond and albedo schemes (both in the Arctic and Antarctic), and ocean mixing coefficients all may be tuned to some degree. Going forward, studies recommend reducing the need for ad-hoc tuning by improving physical realism– for example, ensuring accurate coupling of ice with atmosphere/ocean momentum and heat fluxes (Nie et al., 2023). In Arctic simulations, better coupling (e.g. improved ice–ocean drag and air–ice drag) was shown to reduce sea-ice bias, which may apply in the Antarctic as well.

High snowfall rates on thin sea-ice can lead to snow loading and flooding: the weight of snow depresses the ice floe, allowing seawater to inundate the snow layer, which subsequently freezes into snow-ice. Observations indicate that the snow-ice formation occurs across all Antarctic sectors during the growth season, contributing significantly to total ice thickness (Maksym and Markus, 2008). Climate models that include this process can build additional ice mass on top of the original ice, thickening the ice cover despite the insulating effect of snow. If a model omits or poorly parameterizes snow-ice formation, it will likely underestimate SIT, especially in heavy snowfall regions. At the same time, a deep snowpack insulates the ice from cold air, reducing basal ice growth. The net effect on SIT is a balance: more snow can mean slower growth, but also more snow-ice added. Model sensitivity studies confirm that uncertainties in snow processes strongly affect simulated SIT. For instance, altering the prescribed snow depth or thermal properties can change modeled SIT by about 10cm to nearly a meter (Nie et al., 2023). As mentioned in Sect. 2.1, snow cover is also a key factor in satellite thickness retrievals, which helps explain why models compare differently to satellite observations versus reanalyses in opposite seasons.

627 The presence of model deviations can hamper our understanding of climate-sea-ice interactions as
628 well as biological feedback between the oceans and climate. For instance, due to the existing
629 relationships between SIT and sea-ice motion, biases in the simulated thickness will also affect the
630 dynamics in the models which in turn will impact our understanding of the overall Antarctic sea-
631 ice trends in the models (Lecomte et al., 2016; Sun and Eisenman, 2021). Additionally, lower SIT
632 could create the misleading impression of lower albedo and increased light penetration,
633 subsequently leading to increased Primary Production (Jeffery et al., 2020). Our study does not
634 explore the reasons behind such continued biases in CMIP6. However, there are a variety of
635 potential explanations (besides ones explained above) which may include cloud effects (Kay et al.,
636 2016; Zelinka et al., 2020), spatial resolution that does not permit eddies, which are understood to
637 be highly important for representation of Southern Ocean dynamics (Poulsen et al., 2018; Rackow
638 et al., 2019), models lacking grounded icebergs as landfast ice (Fraser et al., 2023), biases in
639 Southern Ocean stratification (Martinson and Iannuzzi, 1998), and temperature (Luo et al., 2023)
640 and, the lack of coupled ice sheet interactions, which have relevance for the entire Antarctic
641 climate system (Bronselaer et al., 2018; Golledge et al., 2019; Purich & England, 2023).

642

643 ## 5. Conclusions

644 Given the current context of recent extreme sea-ice loss, it is imperative to develop predictions
645 regarding Antarctic sea-ice behavior to enhance our understanding of its future variability and
646 response to climate change. For this we need reliable SIT estimates along with the surface sea-ice
647 variables, to assess the absolute changes in the global sea-ice cover. However, due to the lack of
648 long-term, high-quality observation datasets, assessing Antarctic SIT and its climatic response
649 remains challenging.

650 While GCMs offer a valuable solution to the above challenge, there is an understanding that they
651 do not yet accurately simulate SIT and SIV. However, it is still necessary to see how well they
652 perform even if only to understand where more work is needed. Therefore, despite existing
653 limitations, this study undertook a comprehensive evaluation of Antarctic SIT and SIV by
654 comparing *historical* simulations of 39 CMIP6 model outputs with three different sea-ice products.
655 This comparison demonstrates that models can provide longer timescales of SIT data, which, when
656 compared with observations-based sea-ice estimates (and accounting for their limitations), can
657 enhance our understanding of Antarctic sea-ice. To place the historical findings in a broader
658 climate context, we ~~further~~ examined future projections under the high-emission *SSP5-8.5* scenario
659 (2015–2100). The projections indicate pronounced SIT declines confined primarily to the cooler
660 seasons (winter and spring), whereas SIV and SIA exhibit a persistent, year-round decrease, with
661 negative anomalies intensifying after approximately 2060. These results provided valuable
662 insights into how the observed post-2016 declines may evolve in a warming climate and help link
663 present-day variability to long-term Antarctic sea-ice vulnerability. Notably, the inclusion of
664 simulated SIT and its variability in our analysis also reveals complex and, at times, unexpected
665 behavior that does not always mirror changes in SIA or volume, underscoring the need for a more
666 nuanced understanding of Antarctic sea-ice responses in a warming climate.

667 An accurate modeling of climatological mean sea-ice cover in the GCMs is an initial step and a
668 necessary condition for accurate projections (Holmes et al., 2022). In line with this, our study
669 shows that most CMIP6 models can simulate the timing of annual cycles of all the sea-ice variables
670 much like the sea-ice products. For SIT, the greatest agreement is observed during the maximum

in February, when the Southern Ocean retains the thickest sea-ice, consisting of very thick ice that survives the summer. However, models fail to capture the SIT minima as observed in the satellite products and instead align more closely with the synthesis estimates (GIOMAS and GECCO3), with the minima of both models and synthesis estimates occurring in May. For SIV, the CMIP6 MMM-based annual maxima are lagged by 1 and 2 months compared to the satellite products and GIOMAS, respectively. The closest agreement in the annual cycles between models and sea-ice products is seen in SIA. Despite this alignment, when examined numerically, the models substantially underestimate the annual cycles across all the variables, with relatively lower biases occurring in SIA. Biases in the modeled cycles of SIV and SIA are higher in April-October, with greater inter-model spreads in fall-winter. Conversely, SIT inter-model spreads are higher during November-March but exhibit relatively lower biases compared to the satellite dataset. CMIP6 models continue to simulate negative trends in Antarctic SIT/SIV, contrary to the observed positive trends, until mid-2015. Additionally, we observe positive trends in SIT/SIV during the cooler seasons, which are absent in SIA. These positive trends may be due to intensified seasonal winds during the cooler seasons and further imply that the variability in total sea-ice mass in these months could be influenced by thickness/volume changes. We also examined seasonal variations in sea-ice correlations, showing positive (negative) relationships between SIA and SIT during September (February). Such seasonal covariances suggest that surface sea-ice parameters such as SIA may be weak predictors of SIT. This in turn can have significant implications for our understanding of absolute sea-ice changes in the Antarctic when based solely on SIA. Investigating the reasons for such covariances is outside the scope of this study.

This study compares the SIT biases using the multi-model means, where we show that model results are closer to the reanalysis/synthesis datasets both over both space and time. The spatial variability of sea-ice biases in CMIP6 models highlights certain challenges in accurately capturing both SIT and SIC, especially near the ice edges. Models exhibit greater disagreement in regions influenced by dynamic processes like ice advection, melting, and freezing, while better agreement is seen in areas with multi-year sea-ice and inner ice packs. The variability in SIT biases is found to be closely linked to uncertainties in the model representation of the ice edge, suggesting that improvements in capturing both the dynamic processes and the correct ice edge location could enhance model performance in simulating sea-ice cover in these areas.

While many CMIP6 models simulate spatial SIT patterns similar to the three sea-ice products, they generally tend to underestimate SIT, especially during September. Intriguingly, certain models display anomalously thick sea-ice along the Peninsula and around the sea-ice edges, even greater than the reference dataset. A potential explanation for the observed thick ice in the Weddell can be the presence of fast-ice (i.e., sea-ice pinned to the coast or grounded icebergs). Such thicknesses observed around the Antarctic Peninsula in Fig.9 significantly exceed what is expected from atmospheric heat loss alone, suggesting the presence of fast ice (Fraser et al., 2023). However, we note that the GCMs do not simulate such landfast ice prognostically. Hence, accumulation of thick ice in this region, as depicted in the models, is likely driven by dynamic processes such as winds or drift, leading to ice piling up against the Antarctic Peninsula. Considering the above findings, we anticipate that future studies will investigate these aspects with respect to Antarctic SIT. Addressing such model biases could be initial steps in further improving the representation of dynamic processes in sea-ice, climate, and biogeochemical models, ensuring their accurate predictions. Understanding the biases in sea-ice parameters and physical mechanisms behind these constraints will lead to improvement in the reliability of sea-ice projections and increase confidence in our understanding of what controls the rate of Antarctic sea-ice loss. Therefore, our research

addresses a critical knowledge gap of understanding and modeling of Antarctic SIT and the dynamics involved in shaping its temporal and spatial distributions using the long-term coupled climate simulations.

Author contributions

ST and MR developed the concept of the paper. ST analyzed all the data and wrote the first draft of the paper. WH helped with the methodology and analysis of the CMIP6 modeled data. All authors assisted during the writing process and critically discussed the contents.

Competing interests

The authors declare that they have no conflict of interest.

Data Availability Statement

The satellite products used in the study are available at https://catalogue.ceda.ac.uk/uuid/b1f1ac03077b4aa784c5a413a2210bf5 for Envisat and at https://catalogue.ceda.ac.uk/uuid/48fc3d1e8ada405c8486ada522dae9e8 for CryoSat-2 (Hendricks et al., 2018a, 2018b). The GECCO3 sea-ice thickness data are available at https://www.cen.uni-hamburg.de/icdc/data/ocean/easy-init-ocean/gecco3.html last access: 31 May 2021, Köhl, 2020). The GIOMAS sea-ice thickness data are available at https://psc.apl.washington.edu/zhang/Global_seaice/data.html (last access:26 December 2020, Zhang and Rothrick, 2003). Monthly values of sea-ice concentration from NSIDC are available at https://nsidc.org/data/nsidc-0079/versions/3. All the CMIP6 model datasets are available at ESGF website: https://aims2.llnl.gov/search/cmip6/ (Table S2).

References

Abernathey, R.P., Cerovecki, I., Holland, P.R., Newsom, E., Mazloff, M. and Talley, L.D.: Water-mass transformation by sea ice in the upper branch of the Southern Ocean overturning. *Nature Geoscience*, *9*(8), pp.596-601, 2016.

Behrendt, A., Dierking, W., Fahrbach, E., & Witte, H. (2013). Sea ice draft in the Weddell Sea, measured by upward looking sonars. *Earth System Science Data*, *5*(1), 209–226. https://doi.org/10.5194/essd-5-209-2013

Bronselaer, B., Winton, M., Griffies, S. M., Hurlin, W. J., Rodgers, K. B., Sergienko, O. V., Stouffer, R. J., & Russell, J. L. (2018). Change in future climate due to Antarctic meltwater. *Nature*, *564*(7734), Article 7734. https://doi.org/10.1038/s41586-018-0712-z

Cavalieri, D. J., & Parkinson, C. L. (2008). Antarctic sea ice variability and trends, 1979–2006. *Journal of Geophysical Research: Oceans*, *113*(C7). https://doi.org/10.1029/2007JC004564

Comiso, J. C. (2017). Bootstrap Sea Ice Concentrations from Nimbus-7 SMMR and DMSP SSM/I-SSMIS, Version 3 [Data Set]. Boulder, Colorado USA. NASA National Snow and Ice Data Center Distributed Active Archive Center. https://doi.org/10.5067/7Q8HCCWS4I0R. Date Accessed 04-30-2024.

Döscher, R., Acosta, M., Alessandri, A., Anthoni, P., Arsouze, T., Bergman, T., ... & Zhang, Q. (2022). The EC-Earth3 Earth system model for the coupled model intercomparison project 6. *Geosci Model Dev 15 (7): 2973–3020.*

Eayrs, C., Holland, D., Francis, D., Wagner, T., Kumar, R., & Li, X. (2019). Understanding the Seasonal Cycle of Antarctic Sea Ice Extent in the Context of Longer-Term Variability. *Reviews of Geophysics*, *57*(3), 1037–1064. https://doi.org/10.1029/2018RG000631

Eayrs, C., Li, X., Raphael, M. N., & Holland, D. M. (2021). Rapid decline in Antarctic sea ice in recent years hints at future change. *Nature Geoscience*, *14*(7), 460–464. https://doi.org/10.1038/s41561-021-00768-3

Eyring, V., Gleckler, P. J., Heinze, C., Stouffer, R. J., Taylor, K. E., Balaji, V., Guilyardi, E., Joussaume, S., Kindermann, S., Lawrence, B. N., Meehl, G. A., Righi, M., & Williams, D. N. (2016). Towards improved and more routine Earth system model evaluation in CMIP. *Earth System Dynamics*, *7*(4), 813–830. https://doi.org/10.5194/esd-7-813-2016

Fraser, A. D., Wongpan, P., Langhorne, P. J., Klekociuk, A. R., Kusahara, K., Lannuzel, D., Massom, R. A., Meiners, K. M., Swadling, K. M., Atwater, D. P., Brett, G. M., Corkill, M., Dalman, L. A., Fiddes, S., Granata, A., Guglielmo, L., Heil, P., Leonard, G. H., Mahoney, A. R., … Wienecke, B. (2023). Antarctic Landfast Sea Ice: A Review of Its Physics, Biogeochemistry and Ecology. *Reviews of Geophysics*, *61*(2), e2022RG000770. https://doi.org/10.1029/2022RG000770

Golledge, N. R., Keller, E. D., Gomez, N., Naughten, K. A., Bernales, J., Trusel, L. D., & Edwards, T. L. (2019). Global environmental consequences of twenty-first-century ice-sheet melt. *Nature*, *566*(7742), Article 7742. https://doi.org/10.1038/s41586-019-0889-9

Haumann, F. A., Gruber, N., Münnich, M., Frenger, I., & Kern, S. (2016). Sea-ice transport driving Southern Ocean salinity and its recent trends. *Nature*, *537*(7618), 89–92. https://doi.org/10.1038/nature19101

Hendricks S, Paul S and Rinne E (2018a): ESA sea ice climate change initiative (sea_ice_cci): Southern hemisphere sea ice thickness from the CryoSat-2 satellite on a monthly grid (L3C), v2.0 (https://doi.org/10.5285/48fc3d1e8ada405c8486ada522dae9e8)

Hendricks S, Paul S and Rinne E (2018b): ESA sea ice climate change initiative (Sea_Ice_cci): Southern hemisphere sea ice thickness from the Envisat satellite on a monthly grid(L3C), v2.0 (https://doi.org/10.5285/b1f1ac03077b4aa784c5a413a2210bf5)

Hobbs, W., Massom, R., Stammerjohn, S., Reid, P., Williams, G., & Meier, W. (2016). A review of recent changes in Southern Ocean sea ice, their drivers and forcings. *Global and Planetary Change*, *143*. https://doi.org/10.1016/j.gloplacha.2016.06.008

Holland, M. M., Bitz, C. M., Hunke, E. C., Lipscomb, W. H., & Schramm, J. L. (2006). Influence of the Sea Ice Thickness Distribution on Polar Climate in CCSM3. *Journal of Climate*, *19*(11), 2398–2414. https://doi.org/10.1175/JCLI3751.1

Holland, P. R., Bruneau, N., Enright, C., Losch, M., Kurtz, N. T., & Kwok, R. (2014). Modeled trends in Antarctic sea ice thickness. *Journal of Climate*, *27*(10), 3784-3801.

Holland, P. R., & Kwok, R. (2012). Wind-driven trends in Antarctic sea-ice drift. *Nature Geoscience*, *5*(12), 872–875. https://doi.org/10.1038/ngeo1627

Holmes, C. R., Bracegirdle, T. J., & Holland, P. R. (2022). Antarctic Sea Ice Projections Constrained by Historical Ice Cover and Future Global Temperature Change. *Geophysical Research Letters*, *49*(10), e2021GL097413. https://doi.org/10.1029/2021GL097413

Holmes, C. R., Holland, P. R., & Bracegirdle, T. J. (2019). Compensating Biases and a Noteworthy Success in the CMIP5 Representation of Antarctic Sea Ice Processes. *Geophysical Research Letters*, *46*(8), 4299–4307. https://doi.org/10.1029/2018GL081796

Hou, Y., Nie, Y., Min, C., Shu, Q., Luo, H., Liu, J., & Yang, Q. (2024). Evaluation of Antarctic sea ice thickness and volume during 2003–2014 in CMIP6 using Envisat and CryoSat-2 observations. *Environmental Research Letters*, 19(1), 014067.

Jeffery, N., Maltrud, M. E., Hunke, E. C., Wang, S., Wolfe, J., Turner, A. K., Burrows, S. M., Shi, X., Lipscomb, W. H., Maslowski, W., & Calvin, K. V. (2020). Investigating controls on sea ice algal production using E3SMv1.1-BGC. *Annals of Glaciology*, *61*(82), 51–72. https://doi.org/10.1017/aog.2020.7

Kacimi, S., & Kwok, R. (2020). The Antarctic sea ice cover from ICESat-2 and CryoSat-2: freeboard, snow depth, and ice thickness. *The Cryosphere*, 14(12), 4453-4474.

Kay, J. E., Wall, C., Yettella, V., Medeiros, B., Hannay, C., Caldwell, P., & Bitz, C. (2016). Global Climate Impacts of Fixing the Southern Ocean Shortwave Radiation Bias in the Community Earth System Model (CESM). *Journal of Climate*, *29*(12), 4617–4636. https://doi.org/10.1175/JCLI-D-15-0358.1

Koenig, L., Martin, S., Studinger, M., & Sonntag, J. (2010). Polar Airborne Observations Fill Gap in Satellite Data. *Eos, Transactions American Geophysical Union*, *91*(38), 333–334. https://doi.org/10.1029/2010EO380002

Köhl, A. (2020). Evaluating the GECCO3 1948–2018 ocean synthesis – a configuration for initializing the MPI-ESM climate model. *Quarterly Journal of the Royal Meteorological Society*, *146*(730), 2250–2273. https://doi.org/10.1002/qj.3790

Kumar, A., Dwivedi, S., & Rajak, D. R. (2017). Ocean sea-ice modelling in the Southern Ocean around Indian Antarctic stations. *Journal of Earth System Science*, *126*(5), 70. https://doi.org/10.1007/s12040-017-0848-5

Kurtz, N. T., & Markus, T. (2012). Satellite observations of Antarctic sea ice thickness and volume. *Journal of Geophysical Research: Oceans*, *117*(C8). https://doi.org/10.1029/2012JC008141

Kusahara, K., Hasumi, H., Fraser, A. D., Aoki, S., Shimada, K., Williams, G. D., Massom, R., & Tamura, T. (2017). Modeling Ocean–Cryosphere Interactions off Adélie and George V Land, East Antarctica. *Journal of Climate*, *30*(1), 163–188. https://doi.org/10.1175/JCLI-D-15-0808.1

Langhorne, P. J., Squire, V. A., Fox, C., & Haskell, T. G. (1998). Break-up of sea ice by ocean waves. *Annals of Glaciology*, *27*, 438–442. https://doi.org/10.3189/S0260305500017869

843 Lecomte, O., Goosse, H., Fichefet, T., Holland, P. R., Uotila, P., Zunz, V., & Kimura, N. (2016).
844   Impact of surface wind biases on the Antarctic sea ice concentration budget in climate
845   models. *Ocean Modelling*, 105, 60-70.
846 Li, S., Zhang, Y., Chen, C., Zhang, Y., Xu, D., & Hu, S. (2023). Assessment of Antarctic Sea Ice
847   Cover in CMIP6 Prediction with Comparison to AMSR2 during 2015–2021. *Remote*
848   *Sensing*, *15*(8), 2048. https://doi.org/10.3390/rs15082048
849 Li, S., Huang, G., Li, X., Liu, J., & Fan, G. (2021). An assessment of the Antarctic sea ice mass
850   budget simulation in CMIP6 historical experiment. *Frontiers in Earth Science*, *9*,
851   649743.
852 Liao, S., Luo, H., Wang, J., Shi, Q., Zhang, J., & Yang, Q. (2022). An evaluation of Antarctic
853   sea-ice thickness from the Global Ice-Ocean Modeling and Assimilation System based on
854   in situ and satellite observations. *The Cryosphere*, *16*(5), 1807–1819.
855   https://doi.org/10.5194/tc-16-1807-2022
856 Lindsay, R. W., & Zhang, J. (2006). Assimilation of Ice Concentration in an Ice–Ocean Model.
857   *Journal of Atmospheric and Oceanic Technology*, *23*(5), 742–749.
858   https://doi.org/10.1175/JTECH1871.1
859 Luo, F., Ying, J., Liu, T., & Chen, D.: Origins of Southern Ocean warm sea surface temperature
860   bias in CMIP6 models. *npj Climate and Atmospheric Science, 6(1), 127,* 2023.
861 Maksym, T., & Markus, T. (2008). Antarctic sea ice thickness and snow-to-ice conversion from
862   atmospheric reanalysis and passive microwave snow depth. *Journal of Geophysical*
863   *Research: Oceans, 113(C2).*
864 Maksym, T., Stammerjohn, S., Ackley, S., & Massom, R. (2012). Antarctic Sea Ice—A
865   Polar Opposite? *Oceanography*, 25(3),140–151. https://doi.org/10.5670/oceanog.2012.88
866 Martinson, D. G., & Iannuzzi, R. A.: Antarctic ocean-ice interaction: Implications from ocean
867   bulk property distributions in the Weddell Gyre. *Antarctic sea ice: physical processes,*
868   *interactions and variability*, *74*, 243-271, 1998.
869 Martinson, D. G. (2012). Antarctic circumpolar current's role in the Antarctic ice system: An
870   overview. *Palaeogeography, Palaeoclimatology, Palaeoecology*, *335*, 71-74.
871 Massom, R. A., & Stammerjohn, S. E. (2010). Antarctic sea ice change and variability – Physical
872   and ecological implications. *Polar Science*, *4*(2), 149–186.
873   https://doi.org/10.1016/j.polar.2010.05.001
874 Massonnet, F., Mathiot, P., Fichefet, T., Goosse, H., König Beatty, C., Vancoppenolle, M., &
875   Lavergne, T. (2013). A model reconstruction of the Antarctic sea ice thickness and
876   volume changes over 1980–2008 using data assimilation. *Ocean Modelling*, *64*, 67–75.
877   https://doi.org/10.1016/j.ocemod.2013.01.003
878 Meredith, M., Sommerkorn, M., Cassotta, S., Derksen, C., Ekaykin, A., Hollowed, A., ... &
879   Schuur, E. A. G. (2019). Polar regions. chapter 3, ipcc special report on the ocean and
880   cryosphere in a changing climate.
881 Nie, Y., Li, C., Vancoppenolle, M., Cheng, B., Boeira Dias, F., Lv, X., & Uotila, P. (2022).
882   Sensitivity of NEMO4. 0-SI 3 model parameters on sea ice budgets in the Southern
883   Ocean. *Geoscientific Model Development Discussions*, *2022*, 1-41.Notz, D., &
884   Community, S. (2020). Arctic Sea Ice in CMIP6. *Geophysical Research Letters*, *47*(10),
885   e2019GL086749. https://doi.org/10.1029/2019GL086749
886 Parkinson, C. L., & Cavalieri, D. J. (2012). Antarctic sea ice variability and trends, 1979–2010.
887   *The Cryosphere*, *6*(4), 871–880. https://doi.org/10.5194/tc-6-871-2012

888 Paul, S., Hendricks, S., Ricker, R., Kern, S., & Rinne, E. (2018). Empirical parametrization of
889   Envisat freeboard retrieval of Arctic and Antarctic sea ice based on CryoSat-2: Progress
890   in the ESA Climate Change Initiative. *The Cryosphere*, *12*. https://doi.org/10.5194/tc-12-
891   2437-2018
892 Pellichero, V., Sallée, J.-B., Chapman, C. C., & Downes, S. M. (2018). The southern ocean
893   meridional overturning in the sea-ice sector is driven by freshwater fluxes. *Nature
894   Communications*, *9*(1), 1789. https://doi.org/10.1038/s41467-018-04101-2
895 Poulsen, M. B., Jochum, M., & Nuterman, R. (2018). Parameterized and resolved Southern
896   Ocean eddy compensation. *Ocean Modelling*, *124*, 1–15.
897   https://doi.org/10.1016/j.ocemod.2018.01.008
898 Purich, A., & England, M. H. (2023). Projected Impacts of Antarctic Meltwater Anomalies over
899   the Twenty-First Century. *Journal of Climate*, *36*(8), 2703–2719.
900   https://doi.org/10.1175/JCLI-D-22-0457.1
901 Rackow, T., Sein, D. V., Semmler, T., Danilov, S., Koldunov, N. V., Sidorenko, D., Wang, Q.,
902   & Jung, T. (2019). Sensitivity of deep ocean biases to horizontal resolution in prototype
903   CMIP6 simulations with AWI-CM1.0. *Geoscientific Model Development*, *12*(7), 2635–
904   2656. https://doi.org/10.5194/gmd-12-2635-2019
905 Raphael, M.N., Handcock, M.S. A new record minimum for Antarctic sea ice. *Nat Rev Earth
906   Environ* 3, 215–216 (2022). https://doi.org/10.1038/s43017-022-00281-0
907 Roach, L. A., Dörr, J., Holmes, C. R., Massonnet, F., Blockley, E. W., Notz, D., Rackow, T.,
908   Raphael, M. N., O'Farrell, S. P., Bailey, D. A., & Bitz, C. M. (2020). Antarctic Sea Ice
909   Area in CMIP6. *Geophysical Research Letters*, *47*(9), e2019GL086729.
910   https://doi.org/10.1029/2019GL086729
911 Sallée, J. B., Abrahamsen, E. P., Allaigre, C., Auger, M., Ayres, H., Badhe, R., Boutin, J.,
912   Brearley, J. A., de Lavergne, C., ten Doeschate, A. M. M., Droste, E. S., du Plessis, M.
913   D., Ferreira, D., Giddy, I. S., Gülk, B., Gruber, N., Hague, M., Hoppema, M., Josey, S.
914   A., … Zhou, S. (n.d.). Southern ocean carbon and heat impact on climate. *Philosophical
915   Transactions. Series A, Mathematical, Physical, and Engineering Sciences*, *381*(2249),
916   20220056. https://doi.org/10.1098/rsta.2022.0056
917 Schlosser, E., Haumann, F. A., & Raphael, M. N. (2018). Atmospheric influences on the
918   anomalous 2016 Antarctic sea ice decay. *The Cryosphere*, *12*(3), 1103-1119.
919 Schultz, C. (2013). Antarctic sea ice thickness affects algae populations. *Eos, Transactions
920   American Geophysical Union*, *94*. https://doi.org/10.1002/2013EO030032
921 Schwegmann, S., Rinne, E., Ricker, R., Hendricks, S., & Helm, V. (2016). About the consistency
922   between Envisat and CryoSat-2 radar freeboard retrieval over Antarctic sea ice. *The
923   Cryosphere*, *10*(4), 1415–1425. https://doi.org/10.5194/tc-10-1415-2016
924 Shi, Q., Yang, Q., Mu, L., Wang, J., Massonnet, F., & Mazloff, M. R. (2021). Evaluation of sea-
925   ice thickness from four reanalyses in the Antarctic Weddell Sea. *The Cryosphere*, *15*(1),
926   31–47. https://doi.org/10.5194/tc-15-31-2021
927 Shu, Q., Song, Z., & Qiao, F. (2015). Assessment of sea ice simulations in the CMIP5 models.
928   *The Cryosphere*, *9*(1), 399–409. https://doi.org/10.5194/tc-9-399-2015
929 Shu, Q., Wang, Q., Song, Z., Qiao, F., Zhao, J., Chu, M., & Li, X. (2020). Assessment of Sea Ice
930   Extent in CMIP6 With Comparison to Observations and CMIP5. *Geophysical Research
931   Letters*, *47*(9), e2020GL087965. https://doi.org/10.1029/2020GL087965
932 Singh, H. K. A., Landrum, L., Holland, M. M., Bailey, D. A., & DuVivier, A. K. (2021). An
933   Overview of Antarctic Sea Ice in the Community Earth System Model Version 2, Part I:

Analysis of the Seasonal Cycle in the Context of Sea Ice Thermodynamics and Coupled Atmosphere-Ocean-Ice Processes. *Journal of Advances in Modeling Earth Systems*, *13*(3), e2020MS002143. https://doi.org/10.1029/2020MS002143

Stammerjohn, S., Martinson, D., Smith, R., Yuan, X., & Rind, D. (2008). Trends in Antarctic annual sea ice retreat and advance and their relation to El Niño-Southern Oscillation and Southern Annular Mode variability. *Journal of Geophysical Research: Oceans*, *113*.

St-Laurent, P., Yager, P. L., Sherrell, R. M., Stammerjohn, S. E., & Dinniman, M. S. (2017). Pathways and supply of dissolved iron in the Amundsen Sea (Antarctica). *Journal of Geophysical Research: Oceans*, *122*(9), 7135–7162. https://doi.org/10.1002/2017JC013162

Stroeve, J., Barrett, A., Serreze, M., & Schweiger, A. (2014). Using records from submarine, aircraft and satellites to evaluate climate model simulations of Arctic sea ice thickness. *The Cryosphere*, *8*(5), 1839–1854. https://doi.org/10.5194/tc-8-1839-2014

Sun, S., & Eisenman, I. (2021). Observed Antarctic sea ice expansion reproduced in a climate model after correcting biases in sea ice drift velocity. *Nature communications*, 12(1), 1060.

Tilling, R., Ridout, A., & Shepherd, A. (2019). Assessing the Impact of Lead and Floe Sampling on Arctic Sea Ice Thickness Estimates from Envisat and CryoSat-2. *Journal of Geophysical Research: Oceans*, *124*(11), Article 11.

Trivedi, S., Hobbs, W. R., & Raphael, M. (2024). An Assessment of Antarctic Sea-ice Thickness in CMIP6 Simulations with Comparison to the Observations. *ESS Open Archive eprints*, October 15, 2024. DOI: 10.22541/essoar.171042687.79004452/v2 [Preprint]

Turner, J., Bracegirdle, T. J., Phillips, T., Marshall, G. J., & Hosking, J. S. (2013). An Initial Assessment of Antarctic Sea Ice Extent in the CMIP5 Models. *Journal of Climate*, *26*(5), 1473–1484. https://doi.org/10.1175/JCLI-D-12-00068.1

Turner, J., Hosking, J. S., Bracegirdle, T. J., Marshall, G. J., & Phillips, T. (2015). Recent changes in Antarctic Sea Ice. *Philosophical Transactions of the Royal Society A: Mathematical, Physical and Engineering Sciences*, *373*(2045), 20140163. https://doi.org/10.1098/rsta.2014.0163

Turner, J., Phillips, T., Marshall, G. J., Hosking, J. S., Pope, J. O., Bracegirdle, T. J., & Deb, P. (2017). Unprecedented springtime retreat of Antarctic sea ice in 2016. *Geophysical Research Letters*, *44*(13), 6868-6875.

Turner, J., Holmes, C., Caton Harrison, T., Phillips, T., Jena, B., Reeves-Francois, T., ... & Bajish, C. (2022). Record low Antarctic sea ice cover in February 2022. *Geophysical Research Letters*, *49*(12), e2022GL098904.

Uotila, P., Holland, P. R., Vihma, T., Marsland, S. J., & Kimura, N. (2014). Is realistic Antarctic sea-ice extent in climate models the result of excessive ice drift? *Ocean Modelling*, *79*, 33–42. https://doi.org/10.1016/j.ocemod.2014.04.004

Van Achter, G., Fichefet, T., Goosse, H., Pelletier, C., Sterlin, J., Huot, P.-V., Lemieux, J.-F., Fraser, A. D., Haubner, K., & Porter-Smith, R. (2022). Modelling landfast sea ice and its influence on ocean–ice interactions in the area of the Totten Glacier, East Antarctica. *Ocean Modelling*, *169*, 101920. https://doi.org/10.1016/j.ocemod.2021.101920

Vernet, M., Geibert, W., Hoppema, M., Brown, P. J., Haas, C., Hellmer, H. H., Jokat, W., Jullion, L., Mazloff, M., Bakker, D. C. E., Brearley, J. A., Croot, P., Hattermann, T., Hauck, J., Hillenbrand, C.-D., Hoppe, C. J. M., Huhn, O., Koch, B. P., Lechtenfeld, O. J., … Verdy, A. (2019). The Weddell Gyre, Southern Ocean: Present Knowledge and Future

980   Challenges. *Reviews of Geophysics*, *57*(3), 623–708.
981   https://doi.org/10.1029/2018RG000604

982 Voldoire, A., Saint-Martin, D., Sénési, S., Decharme, B., Alias, A., Chevallier, M., ... &
983   Waldman, R.: Evaluation of CMIP6 deck experiments with CNRM-CM6-1. *Journal of*
984   *Advances in Modeling Earth Systems*, *11*(7), 2177-2213, 2019.

985 Wang, J., Min, C., Ricker, R., Shi, Q., Han, B., Hendricks, S., Wu, R., & Yang, Q. (2022). A
986   comparison between Envisat and ICESat sea ice thickness in the Southern Ocean. *The*
987   *Cryosphere*, *16*(10), 4473–4490. https://doi.org/10.5194/tc-16-4473-2022

988 Willatt, R. C., Giles, K. A., Laxon, S. W., Stone-Drake, L., & Worby, A. P. (2010). Field
989   Investigations of Ku-Band Radar Penetration Into Snow Cover on Antarctic Sea Ice.
990   *IEEE Transactions on Geoscience and Remote Sensing*, *48*(1), 365–372.
991   https://doi.org/10.1109/TGRS.2009.2028237

992 Williams, R. G., Ceppi, P., Roussenov, V., Katavouta, A., & Meijers, A. J. (2023). The role of
993   the Southern Ocean in the global climate response to carbon emissions. *Philosophical*
994   *Transactions of the Royal Society A*, *381(2249),* 20220062.

995 Worby, A. P., Geiger, C. A., Paget, M. J., Woert, M. L. V., Ackley, S. F., & DeLiberty, T. L.
996   (2008). Thickness distribution of Antarctic sea ice. *Journal of Geophysical Research:*
997   *Oceans*, *113*(C5). https://doi.org/10.1029/2007JC004254

998 Xu, Y., Li, H., Liu, B., Xie, H., & Ozsoy-Cicek, B. (2021). Deriving Antarctic Sea-Ice Thickness
999   From Satellite Altimetry and Estimating Consistency for NASA's ICESat/ICESat-2
1000   Missions. *Geophysical Research Letters*, *48*(20), e2021GL093425.
1001   https://doi.org/10.1029/2021GL093425

1002 Zelinka, M. D., Myers, T. A., McCoy, D. T., Po-Chedley, S., Caldwell, P. M., Ceppi, P., Klein,
1003   S. A., & Taylor, K. E. (2020). Causes of Higher Climate Sensitivity in CMIP6 Models.
1004   *Geophysical Research Letters*, *47*(1), e2019GL085782.
1005   https://doi.org/10.1029/2019GL085782

1006 Zhang, J. (2014). Modeling the Impact of Wind Intensification on Antarctic Sea Ice Volume.
1007   *Journal of Climate*, *27*(1), 202–214. https://doi.org/10.1175/JCLI-D-12-00139.1

1008 Zhang, J., & Rothrock, D. A. (2003). Modeling Global Sea Ice with a Thickness and Enthalpy
1009   Distribution Model in Generalized Curvilinear Coordinates. *Monthly Weather Review*,
1010   *131*(5), 845–861. https://doi.org/10.1175/1520-
1011   0493(2003)131<0845:MGSIWA>2.0.CO;2

1012 Zwally, H. J., Comiso, J. C., Parkinson, C. L., Cavalieri, D. J., & Gloersen, P. (2002). Variability
1013   of Antarctic sea ice 1979–1998. *Journal of Geophysical Research: Oceans*, *107*(C5), 9-1-
1014   9–19. https://doi.org/10.1029/2000JC000733

1015

1016

1017
1018
1019
1020
1021 **References for Supporting Material:**
1022

1023 Bader, David C.; Leung, Ruby; Taylor, Mark; McCoy, Renata B. (2019). *E3SM-Project*
1024   *E3SM1.0 model output prepared for CMIP6 CMIP*. Version *YYYYMMDD*[1].Earth
1025   System Grid Federation. https://doi.org/10.22033/ESGF/CMIP6.2294
1026 Cherchi, A., Fogli, P. G., Lovato, T., Peano, D., Iovino, D., Gualdi, S., Masina, S., Scoccimarro,
1027   E., Materia, S., Bellucci, A., & Navarra, A. (2019). Global Mean Climate and Main
1028   Patterns of Variability in the CMCC-CM2 Coupled Model. Journal of Advances in
1029   Modeling Earth Systems, 11(1), 185–209. https://doi.org/10.1029/2018MS001369
1030 Counillon, F., Keenlyside, N., Bethke, I., Wang, Y., Billeau, S., Shen, M.-L., & Bentsen, M.
1031   (2016). Flow-dependent assimilation of sea surface temperature in isopycnal coordinates
1032   with the Norwegian Climate Prediction Model. Tellus A, 68.
1033   https://doi.org/10.3402/tellusa.v68.32437
1034 Danabasoglu, G., Lamarque, J.-F., Bacmeister, J., Bailey, D. A., DuVivier, A. K., Edwards, J.,
1035   Emmons, L. K., Fasullo, J., Garcia, R., Gettelman, A., Hannay, C., Holland, M. M.,
1036   Large, W. G., Lauritzen, P. H., Lawrence, D. M., Lenaerts, J. T. M., Lindsay, K.,
1037   Lipscomb, W. H., Mills, M. J., … Strand, W. G. (2020). The Community Earth System
1038   Model Version 2 (CESM2). Journal of Advances in Modeling Earth Systems, 12(2),
1039   e2019MS001916. https://doi.org/10.1029/2019MS001916
1040 Döscher, R., Acosta, M., Alessandri, A., Anthoni, P., Arsouze, T., Bergman, T., Bernardello, R.,
1041   Boussetta, S., Caron, L.-P., Carver, G., Castrillo, M., Catalano, F., Cvijanovic, I., Davini,
1042   P., Dekker, E., Doblas-Reyes, F. J., Docquier, D., Echevarria, P., Fladrich, U., … Zhang,
1043   Q. (2022). The EC-Earth3 Earth system model for the Coupled Model Intercomparison
1044   Project 6. Geoscientific Model Development, 15(7), 2973–3020.
1045   https://doi.org/10.5194/gmd-15-2973-2022
1046 Gettelman, A., Mills, M. J., Kinnison, D. E., Garcia, R. R., Smith, A. K., Marsh, D. R., Tilmes,
1047   S., Vitt, F., Bardeen, C. G., McInerney, J., Liu, H., Solomon, S. C., Polvani, L. M.,
1048   Emmons, L. K., Lamarque, J., Richter, J. H., Glanville, A. S., Bacmeister, J. T., Phillips,
1049   A. S., … Randel, W. J. (2019). The Whole Atmosphere Community Climate Model
1050   Version 6 (WACCM6). Journal of Geophysical Research: Atmospheres, 124(23), Article
1051   23.
1052 Golaz, J.-C., Van Roekel, L. P., Zheng, X., Roberts, A. F., Wolfe, J. D., Lin, W., et al. (2022).
1053   The DOE E3SM Model version 2: Overview of the physical model and initial model
1054   evaluation. Journal of Advances in Modeling Earth Systems, 14,
1055   e2022MS003156, https://doi.org/10.1029/2022MS003156
1056 Gutjahr, O., Putrasahan, D., Lohmann, K., Jungclaus, J. H., von Storch, J.-S., Brüggemann, N.,
1057   Haak, H., & Stössel, A. (2019). Max Planck Institute Earth System Model (MPI-ESM1.2)
1058   for the High-Resolution Model Intercomparison Project (HighResMIP). Geoscientific
1059   Model Development, 12(7), 3241–3281. https://doi.org/10.5194/gmd-12-3241-2019
1060 Held, I. M., Guo, H., Adcroft, A., Dunne, J. P., Horowitz, L. W., Krasting, J., Shevliakova, E.,
1061   Winton, M., Zhao, M., Bushuk, M., Wittenberg, A. T., Wyman, B., Xiang, B., Zhang, R.,
1062   Anderson, W., Balaji, V., Donner, L., Dunne, K., Durachta, J., … Zadeh, N. (2019).
1063   Structure and Performance of GFDL's CM4.0 Climate Model. Journal of Advances in
1064   Modeling Earth Systems, 11(11), 3691–3727. https://doi.org/10.1029/2019MS001829
1065 Kim, YoungHo; Noh, Yign; Kim, Dongmin; Lee, Myong-In; Lee, Ho Jin; Kim, Sang Yeob;
1066   Kim, Daehyun (2019). KIOST KIOST-ESM model output prepared for CMIP6
1067   CMIP. Version YYYYMMDD[1].Earth System Grid
1068   Federation. https://doi.org/10.22033/ESGF/CMIP6.1922

Lin, Y., Huang, X., Liang, Y., Qin, Y., Xu, S., Huang, W., Xu, F., Liu, L., Wang, Y., Peng, Y., Wang, L., Xue, W., Fu, H., Zhang, G. J., Wang, B., Li, R., Zhang, C., Lu, H., Yang, K., … Gong, P. (2020). Community Integrated Earth System Model (CIESM): Description and Evaluation. Journal of Advances in Modeling Earth Systems, 12(8), e2019MS002036. https://doi.org/10.1029/2019MS002036

Lurton, T., Balkanski, Y., Bastrikov, V., Bekki, S., Bopp, L., Braconnot, P., Brockmann, P., Cadule, P., Contoux, C., Cozic, A., Cugnet, D., Dufresne, J.-L., Éthé, C., Foujols, M.-A., Ghattas, J., Hauglustaine, D., Hu, R.-M., Kageyama, M., Khodri, M., … Boucher, O. (2020). Implementation of the CMIP6 Forcing Data in the IPSL-CM6A-LR Model. Journal of Advances in Modeling Earth Systems, 12(4), e2019MS001940. https://doi.org/10.1029/2019MS001940

Massonnet, F., Ménégoz, M., Acosta, M., Yepes-Arbós, X., Exarchou, E., & Doblas-Reyes, F. J. (2020). Replicability of the EC-Earth3 Earth system model under a change in computing environment. Geoscientific Model Development, 13(3), 1165–1178. https://doi.org/10.5194/gmd-13-1165-2020

Mauritsen, T., Bader, J., Becker, T., Behrens, J., Bittner, M., Brokopf, R., Brovkin, V., Claussen, M., Crueger, T., Esch, M., Fast, I., Fiedler, S., Fläschner, D., Gayler, V., Giorgetta, M., Goll, D. S., Haak, H., Hagemann, S., Hedemann, C., … Roeckner, E. (2019). Developments in the MPI-M Earth System Model version 1.2 (MPI-ESM1.2) and Its Response to Increasing CO2. Journal of Advances in Modeling Earth Systems, 11(4), 998–1038. https://doi.org/10.1029/2018MS001400

Park, S., Shin, J., Kim, S., Oh, E., & Kim, Y. (2019). Global Climate Simulated by the Seoul National University Atmosphere Model Version 0 with a Unified Convection Scheme (SAM0-UNICON). Journal of Climate, 32. https://doi.org/10.1175/JCLI-D-18-0796.1

Seland, Ø., Bentsen, M., Olivié, D., Toniazzo, T., Gjermundsen, A., Graff, L. S., Debernard, J. B., Gupta, A. K., He, Y.-C., Kirkevåg, A., Schwinger, J., Tjiputra, J., Aas, K. S., Bethke, I., Fan, Y., Griesfeller, J., Grini, A., Guo, C., Ilicak, M., … Schulz, M. (2020). Overview of the Norwegian Earth System Model (NorESM2) and key climate response of CMIP6 DECK, historical, and scenario simulations. Geoscientific Model Development, 13(12), 6165–6200. https://doi.org/10.5194/gmd-13-6165-2020

Tang, Q., Golaz, J. C., Van Roekel, L. P., Taylor, M. A., Lin, W., Hillman, B. R., ... & Bader, D. C. (2023). The fully coupled regionally refined model of E3SM version 2: overview of the atmosphere, land, and river results. Geoscientific Model Development, 16(13), 3953-3995.

Tatebe, H., Ogura, T., Nitta, T., Komuro, Y., Ogochi, K., Takemura, T., Sudo, K., Sekiguchi, M., Abe, M., Saito, F., Chikira, M., Watanabe, S., Mori, M., Hirota, N., Kawatani, Y., Mochizuki, T., Yoshimura, K., Takata, K., O'ishi, R., … Kimoto, M. (2019). Description and basic evaluation of simulated mean state, internal variability, and climate sensitivity in MIROC6. Geoscientific Model Development, 12(7), 2727–2765. https://doi.org/10.5194/gmd-12-2727-2019

Vancoppenolle, M., Fichefet, T., Goosse, H., Bouillon, S., Madec, G., & Maqueda, M. A. M. (2009). Simulating the mass balance and salinity of Arctic and Antarctic sea ice. 1. Model description and validation. *Ocean Modelling*, 27(1-2), 33-53.

van Noije, T., Bergman, T., Le Sager, P., O'Donnell, D., Makkonen, R., Gonçalves-Ageitos, M., Döscher, R., Fladrich, U., von Hardenberg, J., Keskinen, J.-P., Korhonen, H., Laakso, A., Myriokefalitakis, S., Ollinaho, P., Pérez García-Pando, C., Reerink, T., Schrödner, R.,

Wyser, K., & Yang, S. (2021). EC-Earth3-AerChem: A global climate model with interactive aerosols and atmospheric chemistry participating in CMIP6. Geoscientific Model Development, 14(9), 5637–5668. https://doi.org/10.5194/gmd-14-5637-2021

Weaver, R., Morris, C., & Barry, R. G. (1987). Passive microwave data for snow and ice research: Planned products from the DMSP SSM/I system. Eos, Transactions American Geophysical Union, 68(39), 769-777.

Wyser, K., van Noije, T., Yang, S., von Hardenberg, J., O'Donnell, D., & Döscher, R. (2020). On the increased climate sensitivity in the EC-Earth model from CMIP5 to CMIP6. Geoscientific Model Development, 13(8), 3465–3474. https://doi.org/10.5194/gmd-13-3465-2020

Yukimoto, S., Kawai, H., Koshiro, T., Oshima, N., Yoshida, K., Urakawa, S., Tsujino, H., Deushi, M., Tanaka, T., Hosaka, M., Yabu, S., Yoshimura, H., Shindo, E., Mizuta, R., Obata, A., Adachi, Y., & Ishii, M. (2019). The Meteorological Research Institute Earth System Model Version 2.0, MRI-ESM2.0: Description and Basic Evaluation of the Physical Component. Journal of the Meteorological Society of Japan. Ser. II, 97(5), 931–965. https://doi.org/10.2151/jmsj.2019-051

Ziehn, T., Chamberlain, M. A., Law, R. M., Lenton, A., Bodman, R. W., Dix, M., Stevens, L., Wang, Y.-P., Srbinovsky, J., Ziehn, T., Chamberlain, M. A., Law, R. M., Lenton, A., Bodman, R. W., Dix, M., Stevens, L., Wang, Y.-P., & Srbinovsky, J. (2020). The Australian Earth System Model: ACCESS-ESM1.5. Journal of Southern Hemisphere Earth Systems Science, 70(1), 193–214. https://doi.org/10.1071/ES19035